Environmental variability at the margin of the South American Monsoon System recorded by a high-resolution sediment record from Lagoa Dourada (South Brazil)

Bernd Zolitschka*[1], An-Sheng Lee[1,2], Daniela Piraquive Bermúdez[3], Thomas Giesecke[3,4]

[1]University of Bremen, Institute of Geography, Germany

[2]National Taiwan University, Department of Geosciences and Research Center for Future Earth, Taipei, Taiwan

[3]Department of Palynology and Climate Dynamics, University of Göttingen, Germany

[4]Department of Physical Geography, Utrecht University, The Netherlands

*Corresponding author: University of Bremen, Institute of Geography, Celsiusstr. 2, 28259 Bremen, Germany (E-Mail: zoli@uni-bremen.de)

ORCID's

BZ: https://orcid.org/0000-0001-8256-0420

ASL: https://orcid.org/0000-0002-5492-1986

DPB: https://orcid.org/0000-0002-7686-8135

TG: https://orcid.org/0000-0002-5132-1061

Keywords: hydroclimate, soil erosion, human impact, XRF scanning, geochemistry, Holocene, 8.2 ka event, Little Ice Age, South American Monsoon System (SAMS)

Abstract

High-resolution geochemical and sedimentological data were analyzed for a lacustrine sediment record from Lagoa Dourada (South Brazil). Four distinctly different depositional processes were determined: (1) Suspension fallout of fine-grained minerogenic particles transferred via fluvial activity dominates the Early Holocene and relates to open grassland in the catchment area; (2) Activation of the karst hydrological system with deposition of massive sand layers indicates increased precipitation at the onset of the Middle Holocene; (3) Minerogenic sediments are replaced by organic deposition due to wetter climatic conditions with the development of forests, which together fostered pedogenesis with the release of dissolved nutrients during the Middle to Late Holocene; (4) Human-induced land-use change caused destabilization of soils in the catchment area with resulting cultural soil erosion between AD 1800 and 1950. These depositional trends are linked to intensity variations of the South American Monsoon System (SAMS). Two century-long climatic events detected by high-resolution XRF scanning data confirm this relationship and probably provide signals of the 8.2 ka event and the Little Ice Age (LIA). Both events document increased rainfall with complex

responses of the environmental system. Our SAMS-induced consequences of past hydroclimatic variability on the environment of South Brazil provide background information for better evaluating model projections of future climate change.

Introduction

Brazil is the country with the second largest forest cover in the world and thus provides an enormous potential for decarbonization initiatives through CO_2 storage in biomass. Moreover, the Amazon and the Atlantic rain forests belong to those regions on Earth with the richest biodiversity (Carnaval et al., 2009; Myers et al., 2000). Moreover, the Atlantic rain forest was and is very important for the economic development of Brazil. Where once forests were growing, there is today rapid industrialization hosting one of the most densely populated regions of South America. Most forests disappeared, with less than 10 % remaining as fragmented woodlands with consequences for regional climate, biodiversity and soil erosion (Freitas, 2011).

Past climate change is not directly recorded in environmental archives but has to be inferred from the result of environmental processes acting under particular climate conditions. Such proxy data are usually imperfect recorders of a small number of often not well constrained climate and environmental variables. In this regard, lake sediments are considered one of the most powerful terrestrial archives of past environmental and hydroclimatic variability. Such paleoenvironmental information is also an important contribution to the understanding of present ecosystems and their stability. Through a large number of proxies, lacustrine sediment records have the potential to characterize the lacustrine system and the catchment area with its natural and anthropogenic processes closely linked to regional hydroclimatic conditions. Due to the scarce occurrence of natural lakes in southern and eastern Brazil, a limited number of long-term environmental histories are obtainable. Palynological investigations are among the most available type of studies for this region. However, they are often conducted on sediments from small wetlands generally lacking precise and high-resolution time control.

With this investigation, we provide new sedimentological and geochemical data to study hydroclimatic variations from a climatically sensitive region in S Brazil. The Atlantic rain forest is a 4000 km long and 100-200 km wide band along the Atlantic coast of Brazil, from tropical Natal in the NE (5 °S) to subtropical Porto Alegre in the S (30 °S). Its appearance is dependent on the spatial and temporal distribution of precipitation and climatologically controlled by the South American Monsoon System (SAMS) (Deininger et al., 2019; Zhou and Lau, 1998). Moreover, this is the most significant atmospheric circulation system of South America and responsible for precipitation from the Amazon to the La Plata Basin (Baker and Fritz, 2015). This large-scale climatic system is driven by differential heating of continents and oceans and responsible for seasonal reversals of low-level winds, a typical monsoon feature (Zhou and Lau, 1998). In southern winter, the Inter-Tropical Convergence Zone (ITCZ) remains north of the equator, while SE Brazil is dominated by the South Atlantic high-pressure cell moving towards the continent. Thus, the advection of cold polar air masses closely linked to South Atlantic cyclones (SACs) brings humidity from the Atlantic Ocean to South America with coastal rainfall from 25-30 °S. At the same time, NE Brazil experiences a dry season of 6-8 months duration. This constellation changes in the southern summer, when the ITCZ extends further to the south. Warm and moist tropical air masses from the Amazon Basin cause rainfall from 15-25 °S, while the Atlantic high-pressure cell is weakened and moves to an offshore position (Baker and Fritz, 2015; Ledru et al., 1998). Currently, 60 % of precipitation is related to the summer monsoon (October-March) and 40 % are considered winter rain (Cruz et al., 2007). Most of the millennial-scale variability of the SAMS coincides with orbital forcing, i.e. variations of insolation, while minor influences are related to the Southern Hemispheric Westerlies (SHW) and Atlantic sea surface temperatures (Baker and Fritz, 2015; Deininger et al., 2019; Utida et al., 2020). As the Atlantic rain forest depends on the amount of precipitation, orbitally controlled changes in precipitation are directly linked to its retractions and expansions but also to changes in vegetation types, i.e. from grassland to forests and vice versa (Ledru et al., 2009; Novello et al., 2017).

The majority of paleoenvironmental investigations carried out in this SAMS-dominated region are mainly pollen and charcoal studies of peat bogs and a small number of studies on lake sediments reconstructing Holocene and Pleistocene vegetation (e.g., Behling, 1995, 2003; Behling and Safford, 2009). So far only three multiproxy studies were carried out that include geochemical, sedimentological, diatom and/or stable isotope data and provide a more comprehensive picture of environmental processes: Lago Aleixo at 18 °S (Enters et al., 2010), Lago Silvana at 19.5 °S (Rodrigues-Filho et al., 2002) and Lagoa Dourada at 25 °S (Melo et al., 2003; Moro et al., 2004). Located at the southern fringe of SAMS influence, Lagoa Dourada is the most interesting. Initial low-resolution investigations are already available including palynology, total carbon, $\delta^{13}C$, LOI-550, selected elements (P, Ca, Mg, K) as well as diatoms. However, the provided chronology is based on only two bulk radiocarbon dates from the Early Holocene insufficient for a detailed understanding of paleoenvironmental changes (Lorscheitter and Takeda, 1995; Melo et al., 2003; Moro et al., 2004).

Thirty years after first investigations at Lagoa Dourada, this lake caught our attention, was re-visited and two overlapping sediment profiles were recovered to (1) obtain a longer record that extends further back in time; (2) apply high-resolution scanning techniques (X-ray fluorescence, magnetic susceptibility) to establish a continuous composite profile; (3) use terrestrial macro remains for radiocarbon dating providing a sophisticated age-depth model; (4) deliver a high-resolution pollen and charcoal record reliably linking vegetation and forest fires to climatic variations and human activities; (5) provide a high-resolution geochemical and sedimentological dataset to determine the responses of involved lacustrine and geomorphological systems to climatic variability and anthropogenic impacts; and (6) investigate the regional hydroclimatic history. This study particularly includes a geochemical characterization of three different sediment sources – lacustrine organic productivity, karstic springs and river floods (Melo et al., 2003; Moro et al., 2004). Except for the pollen study, which is discussed by Piraquive Bermúdez (2020) and will be published elsewhere, this investigation provides a comprehensive and well-dated multiproxy investigation allowing insights into geomorphological processes in the catchment area as well as into limnological processes of the lake, all reflecting hydroclimatic fluctuations in response to SAMS variability during the Holocene.

Study Site

Lagoa Dourada (Portuguese: Golden Lake) is located in Vila Velha State Park near Ponta Grossa (25°14’25” S, 50°02’59” W, 817 m asl) around 80 km W of Curitiba, the capital of the State of Paraná (South Brazil), and 180 km W of the Atlantic coast. The small lake has a maximum water depth of 5.4 m and is elliptical in shape with a size of ca. 150 m x 200 m (Moro et al., 2004). It was formed in the Furnas Formation on the Second Parana Plateau (Fig. 1). The Furnas Formation is of Silurian to Devonian age, part of the Paleozoic Paraná Sedimentary Basin, mainly consists of whitish, medium to coarse-grained quarzitic sandstones (Melo and Giannini, 2007; Pires et al., 2019) and is classified as quartz-arenite with 97 % quartz (Pontes et al., 2020). Aside from mainly kaolinite as cement, these sandstones are enriched in ultra-stable minerals such as zircon (Moro et al., 2004). Chemical weathering of the cement as well as of quartz-grain surfaces by intergranular corrosion is responsible for the process of arenization, which loosens and removes sand grains by groundwater (Wray, 2013). Overall, arenization increases the underground porosity and finally causes the development of silicate karst.

The Vila Velha State Park was created in 1953 and is enlisted as a State Heritage since 1966 (Thomaz, 2010). It is famous for its karstic features in sandstone with caves, dolines, sinkholes, speleothems, karren, collapse structures and underground drainage systems including karstic springs (Melo and

Giannini, 2007). The formation of quarzitic karst is very slow-acting compared to carbonaceous karst and requires extended periods of geological stability with intensive chemical weathering. As a consequence of subterranean karstic erosion, Lagoa Dourada was formed as a sinkhole after the roof of a cave collapsed. Such sinkholes (Portuguese: furnas) are typical for this part of the Paraná Basin and eponymous for the Paleozoic Furnas Formation.

As the non-fluvial catchment area of Lagoa Dourada is composed of siliceous karst, there is limited surface runoff into the lake: precipitation immediately infiltrates, contributes to the underground karstic drainage system and returns to the surface via layered karstic springs at the northern shores of Lagoa Dourada. There the Furnas Formation borders the alluvial plain of Rio Guabiroba. Petrographic data document that sands transferred via karstic springs are enriched in ultra-stable minerals like their source: the Furnas Formation (Melo et al., 2003).

The short and ca. 300 m-long outflow of Lagoa Dourada drains into Rio Guabiroba. However, during wet seasons with flooding, the water in the outflow channel changes direction and enters the lake. These floodwater invasions are silting-up Lagoa Dourada from the south, while the largest water depth of the lake is close to the northern shore (Melo et al., 2003). During flooding, a much larger catchment area extends ca. 25 km towards the east (Fig. 1). This watershed of Rio Guabiroba includes not only sandstones of the Furnas Formation but also shales and fine-grained sandstones of the Devonian Ponta Grossa Formation as well as reddish and predominantly medium-grained Vila Velha sandstones of the Upper Carboniferous Itararé Group (Fig. 1). The latter is cemented by iron and manganese oxides and dominated by quartz with a high mineralogical maturity (Melo et al., 2003; Melo and Coimbra, 1996). Some of the strongly cemented parts of the Vila Velha sandstone are resistant against weathering and form ruined inselbergs described as “ruiniform relief” (Melo and Coimbra, 1996), one of the major attractions of the Vila Velha State Park.

The subtropical climate at Vila Velha is characterized by temperate oceanic conditions (Cfb according to the Köppen classification) without dry seasons. The mean annual temperature is 17.5 °C (warmest month January: 21.4 °C; coldest month July: 13.7 °C) and the annual sum of precipitation reaches 1495 mm (wettest month February: 177 mm; driest month August: 83 mm) (Merkel, 2020). Regional vegetation is dominated by subtropical grassland (Campos) with *Araucaria* woodlands covering hills and valleys (Moro and Fürstenberger, 1998). A recent vegetation map of the Vila Velha State Park determined *Araucaria angustifolia* (12 %) as the characteristic local tree in valleys and moister habitats with deeper soils, while on shallow and drier soils on sandstones Campos dominates with Poaceae (23 %), Cyperaceae (13 %), Asteraceae (10 %) and *Baccharis* (9 %) (Piraquive Bermúdez et al., 2021).

The modern freshwater of Lagoa Dourada is characterized by alkalinity of 77.5 mg/l, pH of 7.8, water temperature of 19.8 °C and 9.2 mg/l dissolved oxygen. All measurements are mean August values obtained from the epilimnion of 1990-1993 (Moro and Fürstenberger, 1998). These water conditions are confirmed by modern diatom samples, which document eutrophic conditions typical for a shallow alkaline to neutral lake with a dominance (>90 %) of periphytic over planktonic diatom species (Moro and Fürstenberger, 1998).

Methods

Coring, lithological description and subsampling

In February 2017 two parallel and overlapping sediment cores (LD17-A: to a sediment depth of 14.0 m; LD17-B: 14.2 m) have been recovered. The upper 10 m were cored with a light-weight Livingstone piston corer (Nesje et al., 1987) and the deeper sediments with a square-rod Livingstone piston corer (Wright, 1967). The 1 m long core sections (diameter: 50 mm) were obtained from a location south of the largest water depth (5.4 m) of Lagoa Dourada (50°2'58.21" W; 25°14'25.55" S). Coring sites were 10-15 m apart and at 4.0 m (LD17-A) and 2.8 m (LD17-B) water depths (Fig. 1). The upper 20 cm of the record were almost liquid, difficult to retain and only used for pollen analysis. All sediment cores were shipped to the University of Göttingen, where they were split, photographed and described macroscopically. In addition, 14 smear slides from characteristic intervals were prepared following Rothwell (1989) for microscopic sediment description (magnification: 100-400 x) at the University of Bremen. In support of core description, high-resolution color images were available from the line-scan camera mounted to the ITRAX X-ray fluorescence (XRF) core-scanner (Croudace et al., 2019; Croudace et al., 2006).

Subsampling for pollen (Piraquive Bermúdez, 2020) and in parallel for sedimentology and geochemistry (this study) was carried out providing a total of 177 samples with a mean spatial resolution of 8 cm.

Dating

Terrestrial plant macro remains, encountered during subsampling and searched for by sieving sediment slices, were preferably used for radiocarbon dating wherever possible. However, no macroscopic plant remains were found below 7,4 mcd, except for a part of a twig at 9,25 mcd. Twenty-one AMS ^{14}C samples were dated at the Poznań Radiocarbon Laboratory in Poland (POZ) and two additional samples at the ^{14}Chrono Centre, Queen's University Belfast in Northern Ireland (UBA). Eight dates derive from terrestrial plant macro remains, while the other determinations are based on bulk organic matter (OM; Tab. 1). To assess the magnitude of a presumed old carbon effect of bulk dates (reservoir effect), two sediment samples were submitted for radiocarbon dating above and below the terrestrial macrofossil date at 7,31 mcd. These two dates were not used in building the age model. In addition to the radiocarbon dates, the sediment/water interface (AD 2017) is used as a control point, while distinct sand sections in the core are interpreted as events and treated as instantaneous. Sediment accumulation in relation to the results of radiocarbon measurements and the core top was modelled using the R-package "rbacon" (Blaauw et al., 2021). Radiocarbon dates were calibrated during age modelling applying the Southern Hemisphere calibration curve SHCal20 (Hogg et al., 2020).

Several publications used for discussion provide only uncalibrated radiocarbon ages. To improve comparisons with our data, these ages were calibrated using OxCal 4.4 (Bronk Ramsey, 2009) applying the Southern Hemisphere calibration curve SHCal20 (Hogg et al., 2020).

Core scanning

Prior to applying non-destructive core scanning techniques, the split core halves were cleaned and smoothened. A continuous log of volume-specific magnetic susceptibility (MS) was measured in 1 cm increments with a Bartington MS2E sensor employed to an automated measuring bench (Dearing, 1994; Nowaczyk, 2001). For analyzing the geochemical composition of sediment cores in high resolution, all sections were scanned with the ITRAX XRF core scanner (Cox Analytics) (Croudace et al., 2019; Croudace and Rothwell, 2015). The molybdenum (Mo) tube was used with constant settings of 30 kV and 50 mA, a step size of 2 mm and an exposure time of 5 s. The output was processed with the software Q-spec (Cox Analytics) and results are expressed in counts (cts), which describe relative intensities of 23 elements as well as variations of coherent (coh) and incoherent (inc) scattering.

In a next step, reproducibility of XRF elemental data was evaluated by five repeated scans of two 1 m long sections representing highly organic (sediment core LD17-B6) and highly minerogenic (LD17-B12) sediment with the same adjustments as mentioned above. A feasible way to evaluate the credibility of each determined element is to calculate correlation coefficients for elements between replicate measurements where high correlations indicate good reproducibility for the respective element. This procedure allows excluding elements with low signal-to-noise ratios (Löwemark et al., 2019), thus reducing the number of elements for statistical evaluation.

Due to changing physical properties along the sediment record, matrix effects related to variations in water content, OM content and/or grainsize, the chemical composition obtained by XRF core scanning is non-linearly correlated to element concentrations (Croudace et al., 2019; Tjallingii et al., 2007). Moreover, element intensities underlie the closed-sum effect, which inhibits multivariate statistical analyses (e.g., Martin-Puertas et al., 2017). A solution for these limiting factors is available with the centered log-ratio (clr), which normalizes data and determines relative changes in element composition resembling their chemical composition (Tjallingii et al., 2007; Weltje et al., 2015; Weltje and Tjallingii, 2008). Moreover, clr transformation is consistent with the statistical theory of compositional data analyses (Aitchison, 1982; Weltje et al., 2015) and calculates as:

clr of $I_{ij} = \ln (I_{ij} / gm_j)$,

where I_{ij} is the intensity (I) of the element i for measurement j and gm_j is the geometric mean of all elements analyzed at measurement j. In addition to elemental clr values, we calculate the log molybdenum incoherent/coherent scattering ratio (ln inc/coh), which is regarded as a proxy for OM content of lacustrine sediments (Liu et al., 2013; Woodward and Gadd, 2019). This ratio of Compton scattering (inc) versus Rayleigh scattering (coh) depends on the presence of light elements (H, C, N, O). High amounts of these elements, such as analyzed for OM and/or high-water content, increase the Compton Effect and thus the value for ln inc/coh. Other possible matrix effects are negligible (Weltje and Tjallingii, 2008; Woodward and Gadd, 2019).

<u>Elemental analyses</u>

Total carbon (TC), total nitrogen (TN) and total sulphur (TS) were measured with a CNS elemental analyzer (EuroEA, Eurovector). Prior to measurements, all 177 samples were freeze-dried, ground, homogenized and 5-20 mg were weighted into tin crucibles. During measurements, the elemental analyzer combusts the crucibles with the sample material at a temperature of 1800 °C. All OM is oxidized and the resulting gases (CO_2, NO_2, SO_2) are detected by chromatography. As TC includes organic as well as inorganic carbon, a second step is necessary to distinguish total organic carbon (TOC) from total inorganic carbon (TIC). As the catchment area has no carbonaceous rocks, we assume that also the lacustrine sediments are carbonate-free. To test this hypothesis, 10 samples with TC values >2 % were treated first with 3 % and then with 20 % HCl at 80 °C to remove potential carbonates prior to measurement of TOC with the same elemental analyzer. Total inorganic carbon (TIC) was then calculated as the difference between TC and TOC. Furthermore and to distinguish autochthonous from allochthonous sources of OM, C/N ratios were calculated with low values (<10) indicative of autochthonous lacustrine productivity (algal matter), while higher values (>20) are dominated by higher plants with cellulose of terrestrial origin (Meyers and Teranes, 2001).

Biogenic silica (BSi) was analyzed for 177 samples following the leaching method of Müller and Schneider (1993). We extracted BSi with 1M NaOH at 85 °C. The solution was cycled by a continuous-flow system into an auto analyzer, where dissolved silicon was detected by spectrophotometry.

<u>Grainsize</u>

Prior to grainsize analysis, OM was removed by H_2O_2 from each of the 177 samples. For dispersion, 20 ml of Calgon [$(NaPO_3)n$] was added and agitated overnight. On the next day analyses were performed with a laser diffraction analyzer (Beckman Coulter LS 200) after ultrasonic treatment for 30 s. Each sample was measured at least four times for 60 s until a stable distribution was reached. Thereafter, the arithmetic mean was calculated for the best three sample runs. Grainsize distributions and all statistical grainsize parameters were calculated from the output of the LS200 as geometric graphical measures according to Folk and Ward (1957) with the MS Excel-based macro Gradistat, Version 8.0 (Blott and Pye, 2001).

Multivariate statistics

Principal component analysis (PCA) was applied to the standardized and normalized (clr-transformed) dataset obtained by XRF core scanning for reducing the data dimension (Abdi and Williams, 2010). The standardization rescaled each element's profile to zero mean and unit standard deviation. The selection of credible principal components (PCs) is based on the elbow concept and preference is given to PCs with >10 % of total variance. The first two PCs were selected and whitened (i.e., standardized) as data representation. The logic of whitening is the same as for standardization prior to PCA. The process of whitening gives the two selected PCs equal contribution for later clustering. We applied "hierarchical density-based spatial clustering of applications with noise" (HDBSCAN). This clustering algorithm combines hierarchical clustering with the spatial density metric of data and tends to find clusters with dense distributions (McInnes et al., 2017). Due to density-based characteristics, the shapes of the clusters are not limited to sphere-like shapes but can also be polygons as long as data points within these clusters are dense enough. Furthermore, data points located in a loose manner or at distance from the cores of dense clusters will be recognized as noise, i.e. outlying data. This makes the algorithm robust against noise. HDBSCAN's hierarchical clustering approach on density metric provides flexibility with regard to density. In other words, data points determined as dense clusters can be based on different densities, for details see the algorithm's source documents (https://hdbscan.readthedocs.io/en/latest/index.html). Two primary parameters have to be adjusted for this algorithm. Min_cluster_size sets the minimum size for the grouping of data considered as a cluster and Min_sample determines what the algorithm defines as "dense", i.e. how many data points will be selected as noise. A grid search for optimal parameters (min_cluster_size: 20, 50, 80, 100, 150, 200; min_sample: 2, 3, 4, 5, 8, 10) was carried out by checking the visualization of spatial data distributions on the first two PCs. Optimal min_cluster_size and min_sample were set to 100 and 5, respectively. Computations and part of visualizations were conducted using the packages in the Scipy ecosystem (Harris et al., 2020; Hunter, 2007; Pedregosa et al., 2011; van der Walt et al., 2014; Virtanen et al., 2020) and the HDBSCAN library (McInnes et al., 2017).

Individual cluster labels were smoothed to develop the clusterlog. This was carried out by looking at subsets of 11 consecutive data points (11 x 2 mm). For each of these subsets, fragmented labels and labels of minor importance were replaced by the dominant label. Thus, 31.4 % of noise was changed to cluster labels, which increased the number of cluster labels for all clusters except for cluster 3, which remained unchanged.

Results

Core correlation and lithological description

Correlation of core sections from LD17-A and LD17-B is based on 20 marker layers clearly distinguishable on high-resolution line-scan images and supported by high-resolution XRF core scanning data. Of all detected elements, Ca is best suited for this purpose due to relatively high counts combined with sufficient variability along the entire record (Fig. S1). All depths of the established composite record are provided in meter composite depth (mcd). Technical gaps due to coring typically occur between individual core sections and were bridged down to 10.5 mcd by parallel and overlapping cores (Fig. 2). Beyond 10.5 mcd and until the basal depth of 14.4 mcd there are five intersections of which four could not be bridged due to lacking overlap. These gaps were assumed to be 3 cm wide based on the mean width of similar technical gaps observed in the upper 10 m.

Initially, the scans of magnetic susceptibility (χ) were intended for core correlation. However, the variability of χ was too low for this purpose (Figs. 3, S2). Moreover, above 9.7 mcd LD17-A and LD17-B show mean values for χ of -4.14 SI and -3.98 10^{-6} SI, respectively, i.e. in the field of diamagnetism. Only below 9.7 mcd χ has positive mean values of 7.51 10^{-6} SI for LD17-A and 15.43 10^{-6} SI for LD17-B, i.e. in the field of paramagnetism (Fig. S2). Thus, the record of Lagoa Dourada carries no ferromagnetic signal.

A test for total inorganic carbon (TIC) was carried out with ten samples (supplementary data). The detected values vary around 0 % TIC (mean: 0.4 % TIC) confirming our assumption that the sediment is free of carbonates like the catchment area.

Based on macroscopic as well as on microscopic sediment characterization and supported by bulk geochemistry and grainsize, the sediment record of Lagoa Dourada is subdivided into seven lithological units (lithozones A to G: LZ A-G) with six subzones (Figs. 2, 3). Basal LZ A1 (14.4-12.1 mcd) is a dark gray mud composed of up to 15 % BSi (opal of small planktonic central and pennate diatoms as well as of sponge spicules) but low amounts of TOC (~3 %) in a silt-rich matrix. The C/N ratio decreases from base (15) to top (10) of LZ A1, indicating increasing autochthonous OM supply. This development is interrupted by a gray layer of fine sand (LZ B1: 12.1-12.0 mcd) with almost no organic components. The following LZ C consists of laminated and diatomaceous dark gray mud (12.0-11.5 mcd) with dominating pennate and very small (planktonic) diatoms. C/N ratios remain low (7-12) and medium silt dominates the grainsize. Altogether, this evidences the development of a deeper lake system with peaking BSi (up to 30 %) and increasing TOC values (~5 %). LZ B2 (11.5-10.4 mcd) is a thick and structureless gray sand layer without organic components interrupted by lacustrine deposition. With LZ A2 (10.4-10.0 mcd) the dark gray mud of LZ A1 returns. However, geochemical data show a marked decrease in diatoms (BSi <3 %), while TOC increases to 7 % including more allochthonous organic material as indicated by rising C/N ratios. We interpret this development as a decrease in water depth with less lacustrine and more catchment derived OM. With the third intercalation of gray sand (LZ B3: 10.0-9.5 mcd) inorganic conditions recur with BSi and TOC documenting almost absence of OM.

With the advent of LZ D1 (9.5-8.9 mcd), sediments change markedly (Fig. 3). The bedded brown organic mud differs distinctly from all lithozones below. A color change to brownish hues indicates an increased importance of OM (mean TOC ~10 %) including plant macrofossils explaining the rise of C/N ratios to 32. Diatoms show comparable values (~3 % BSi) like in LZ A2. In addition to changes in color and OM, mean grainsize coarsens from dominance of medium silt in lithozones A and C to coarse silt in LZ D with frequent intercalations of fine sand. LZ D1 is followed by an intercalation of 1.2 m of dark gray sand (LZ E1: 8.9-7.7 mcd) consisting mainly of fine sand without organic components. Following this sand layer, sediments continue with LZ D2 (7.7-6.7 mcd) and increasing TOC values (20 %). Diatoms remain at lower values (~3 % BSi) like before, while C/N ratios decrease to 20. After a second dark gray and fine sand horizon without organic components (LZ E2: 5.7-5.3 mcd), bedded brown organic mud (LZ D3: 5.3-1.1 mcd) continues with increasing OM contents (maxima up to 30 % TOC) and slightly more diatoms (~5 % BSi), while C/N ratios decrease to 13. Throughout LZ D the mean grainsize remains in the coarse silt fraction, while organic productivity increases as documented by higher TOC and BSi values. At the beginning of LZ D3 the influence of allochthonous OM is still high (C/N >20) but decreases thereafter to <15. In LZ D3 amorphous OM is ubiquitous as well as pyrite, which often forms microscopically detectable framboids.

With LZ F (1.1-0.4 mcd) minerogenic sediments recur (Fig. 3). This almost to pale brown clay-rich mud displays a drop in lacustrine productivity to 2 % BSi and 13 % TOC (Fig. 3). Additionally, C/N ratios decline reaching low values of 11, thus indicating dominance of autochthonous OM. Grainsize changes to finest values of the record with a mean in the fine silt fraction and up to 33 % of clay. Finally, at the top of the record there is black, organic-rich and homogenous mud (LZ G: 0.4-0.2 mcd) with a higher water content and TOC values reaching 29 %, while the C/N ratio remains at ~10. Despite these productive conditions causing highly organic sediments, BSi remains <3 %.

XRF scanning data: comparing litholog with clusterlog stratigraphies

The XRF scanner detected 20 elements (Al, Si, P, S, Cl, K, Ca, Ti, V, Cr, Mn, Fe, Ni, Cu, Zn, Br, Rb, Sr, Zr, Pb) with counts varying from 7 (Cl) to 21,607 (Fe) as well as coherent (coh) and incoherent (inc) radiation. Many of the elements have low signal-to-noise ratios and need to be excluded from further discussion. Five replicate XRF scans were carried out for 97 cm of organic sediment from LD17-B6 (LZs D2, E2 and D3) and 97 cm of minerogenic sediment from LD17-B12 (LZs A1, B1 and C). These records were used in correlation analyses to inform on the replicability of the signals. High correlations reveal a generally good reproducibility of elemental analyses (Tab. S1). Only elements with a high positive correlation ($r > 0.8$) for at least one of the two sediment sections scanned are considered for further discussion. Thus, ten elements (Si, S, K, Ca, Ti, Fe, Zn, Rb, Sr, Zr) as well as the inc/coh ratio are selected for principal component analysis (PCA) and cluster analysis (Tab. S1).

The first two principal components (PCs) are representing 64.6 % of the explained total variance (Fig. 4). Additional PC's explain <10 % and were not considered based on the elbow concept (Fig. S3). We interpret the first PC with 43.8 % of explained variance as discriminating between organic (positive direction) and minerogenic sediment composition (negative direction). The second PC with 20.8 % of explained variance represents mainly the trends in grainsize variability with larger grainsizes related to the positive direction and smaller grainsizes to the negative direction. Hierarchical density-based spatial clustering of applications with noise (HDBSCAN) provides four distinct clusters (Fig. 4), which are transferred into a clusterlog to be compared with the litholog (Fig. 2). Although the number of clusterlog units (4) is smaller than the number of litholog units (7), an overall agreement is evident. The discrepancies, i.e. merging of the LZs A with C, B with E as well as D with G, are related to XRF analyses capturing only heavier elements than Al. Thus, changes in organic sediment components consisting of lighter elements such as H, C and O are not detected.

Cluster 1 combines LZ B (gray sand) with LZ E (dark gray sand), the latter being influenced by organic-rich pore water available from under- and overlying highly organic sediments of LZ D. The distinct link to Si and Zr relates these two sandy lithozones to weathering resistant minerals (quartz, zircon) of the Furnas Formation as their source rock. LZ A (dark gray mud) and LZ C (laminated and diatomaceous dark gray mud) together are related to cluster 2, which shows K, Ti and Rb as dominant siliciclastic elements. These elements likely originate from the Ponta Grossa Formation consisting of shales as potential source rocks. Cluster 3 links to LZ F (reddish brown clay-rich mud) with Fe and Sr as dominant elements. As Fe is lacking in the Furnas Formation, these sediments derive from the iron cement of the Vila Velha sandstone. Moreover, PC loadings of Fe plot at the transition from minerogenic to organic components (Fig. 4), which indicates that Fe is not only bound to detrital silicates but also occurs as pyrite (FeS) and thus can as well be related to organic productivity. Sulphur is introduced to the sediment via lacustrine production of OM, which is deposited, decomposed and combines with dissolved Fe under anoxic (reducing) conditions typical for eutrophic lakes. Thus, there is a positive correlation between both elements for organic LZ D ($r = 0.49$). However, the correlation for minerogenic LZs A and C is negative ($r = -0.48$). This characteristic of Fe results in absence of any correlation between Fe and S if the entire record is considered ($r = -0.20$).

In cluster 4, including LZs D (bedded brown organic mud) and G (black, organic-rich homogenous mud), the organic components S, Ca and the inc/coh ratio are combined. Despite this link to cluster 4, Ca has a positive correlation with the siliciclastic elements K ($r = 0.68$), Fe (0.50), Rb (0.68) and Sr (0.75) for LZs A1 and C. More dominantly than Fe, Ca is related to organic productivity, which might be the result of precipitation of calcite from the water column or via carbonaceous shells, which have been observed sporadically and only during coring. However, evidence for carbonate is lacking – TIC was not detected and XRD analysis is not promising because of the very low calcite concentrations, as it was similarly documented for the highly organic sediment record from Laguna Azul (Zolitschka et al., 2019). Finally, the inc/coh ratio has a positive correlation (r = 0.88) with TOC (Fig. S4) and thus provides a very high-resolution record of OM for the sediment record of Lagoa Dourada.

XRF scanning data: stratigraphy of selected elements

High-resolution XRF core-scanning data support the lithological description. However, and due to their high spatial resolution of 2 mm, XRF records are more detailed and provide additional insights. All sand layers are reflected by distinct lows of the ln inc/coh ratio as well as by pronounced peaks of Si (Fig. 5), both proxies clearly document inorganic quartz deposition. The high-resolution OM proxy (ln inc/coh) displays a steady increase of organic productivity from the base of LZ A1 until the top of the record, if the sand layers and LZ F are taken out of consideration. However, a marked increase is observed at the onset of LZ D1, when dark gray mud changes to brown organic mud. This distinct sedimentological transition is even more pronounced in the S record, with low values prior to LZ D1 and much higher values after this transition (Fig. 5). Moreover, after this major sedimentological transition S covaries with Fe, which is explained by diagenetic formation of pyrite (FeS), a mineral that is formed under anoxic conditions and was determined by microscopic smear slide investigation. Such conditions also explain the higher degree of OM preservation during LZ D. During LZs A and C, Fe displays a decreasing trend and no covariation with S. Thus, we consider Fe as being related to a siliciclastic source for this older part of the record. This assumption is supported by the elements K and Ti. Both are siliciclastic and decrease as well during LZs A and C (Fig. 5).

The only marked change in the upper 5 m of the sediment record is related to LZ F: the reddish-brown clay-rich mud. During this lithozone, organic parameters ln inc/coh and S drop to distinctly lower values while Fe increases. We consider this as the result of an increased siliciclastic origin of Fe during LZ F, which is again supported by K and Ti values rising in parallel. In topmost LZ G, most elemental parameters seem to continue from where LZ D3 was interrupted by LZ F. Only the element K shows an unexpected increase during this lithozone peaking at higher values than during entire LZ D.

Grainsize statistics and sediment dynamics

Grainsize analysis documents two distinctly different populations (Fig. 6). Silty sand and fine to medium sand of LZs B and E are moderately well-sorted, unimodal and with one maximum in the fine sand fraction (Fig. S5). The other lithozones except LZ D3 consist of poorly sorted sandy silt or silt. They are characterized by bimodal grainsize distributions (Fig. S5) with maxima in medium to coarse silt fractions and in the fine sand fraction (LZs A1 and F). Only LZ D3 displays a trimodal grainsize distribution with a broad maximum in the fine silt fraction and two narrow maxima in fine and medium sand fractions (Fig. S5).

As there are no dunes or sand sheets in the catchment area to explain the moderately well-sorted sands of LZs B and E, we consider that this distinct unimodal grainsize distribution is inherited from sandstones of the Furnas Formation. During its relatively rapid flow through the karst hydrological system, the groundwater adds no additional grainsize fractions prior to deposition in Lagoa Dourada. Very different from the sand layers, the silt-sized sediment of LZs A, C and F probably originate from the shales of the Ponta Grossa Formation in the catchment area, which is drained via Rio Guabiroba and enters the lake during flooding events where it settles out of suspension. As this suspension freight needs to be transported towards the lake against the slope of the outlet channel (Fig. 1), it is unlikely that the fine sand component observed by the secondary grainsize maximum rained out of suspension from river floods as well. Instead, we consider these sands as subordinated contribution from karstic springs, contributions which are coarser and more pronounced during LZs A and D compared to LZs C and F. Lithozone F has distinctly less fine sand, while there is a four-times higher contribution of clay interpreted as the result of increased soil erosion in the catchment area. This assumes that clay was produced by chemical weathering and pedogenesis of shales from the Ponta Grossa Formation.

Grainsize distributions provide insights into depositional processes at Lagoa Dourada. The two different sand horizons (LZs B and E) can only be differentiated by their color (Fig. 2), but have comparable unimodal grainsize distributions (Fig. S5) and an almost identical chemical composition (Figs. 4, 5). Based on the lack of OM and iron as well as on grainsize and chemical composition inherited from weathering-resistant minerals of the Furnas Formation, we consider these sands as event deposits related to flushing of the karst hydrological system. These sediments are added to the stratigraphic record in relatively short time intervals and thus are without temporal significance for the stratigraphic record. The other lithozones are dominated by silt-sized grainsize fractions, derived from suspension fallout, but also show a minor sandy component (bimodal grainsize distribution, Fig. S5) likely added by karstic springs. This sand component is least pronounced for LZs C and F. The highly organic LZ D shows a trimodal grainsize distribution (Fig. S5) with two maxima in the sand fraction, which is interpreted in terms of increasing importance of the karst system for the contribution of minerogenic components to the lake, while settling out of suspension was reduced.

<u>Age-depth model</u>

All radiocarbon dates from terrestrial macrofossils are in stratigraphic order and their age-depth relationship is almost linear (Tab. 1, Fig. 7). Radiocarbon age determinations on bulk sediment also follow a linear age-depth trend with a cluster of three dates being too young and two dates being too old compared to the trend indicated by the other ten bulk dates. The two radiocarbon dates on bulk sediment above and below the terrestrial macrofossil at 7,3 mcd are too old by 5065 and 5235 radiocarbon years, respectively (Tab. 1). The resulting average of 5150 years was used as an offset applied to all bulk dates prior to calibration. Describing the uncertainty of this reservoir correction, an error of 100 years was added as contribution of old carbon to the sediment, which cannot be regarded as constant with time.

The resulting age-depth model suggests an age between 10,000 and 10,700 cal. BP for the basal sample (Fig. 7). The two aforementioned clusters of five bulk dates deviating from the general trend were not considered by the age model. It is noticeable that four out of five bulk dates deviating from the linear trend are from sand sections. The radiocarbon date of the twiglet at 9,25 mcd was also compared to a neighboring bulk date resulting in an offset of 5145 years (Tab. 1), which confirms that the reservoir effect applied (5150 years) is applicable also for the older part of the record with a much lower OM content.

Interpretation

Processes of sediment formation at Lagoa Dourada are differentiated into three modes according to their elemental composition (Figs. 3, 5) and supported by cluster analysis (Fig. 4). The three involved depositional processes relate to (1) fluvial activities of Rio Guabiroba, (2) discharge through the karst hydrological system and (3) autochthonous lacustrine productivity. The contribution of all three processes varies through time. However, one of them can always be regarded as the leading depositional process. Prevalence of karstic runoff is considered for the five sand layers, i.e. cluster 1 (Figs. 2, 4). As coarse-grained deposits they differ from the fine-grained silts related to seasonal flooding of the river. Therefore, they are regarded as short events and thus as stratigraphically insignificant. Therefore, these intercalations via karst hydrology are excluded from the discussion of past environmental conditions as well as from the selection of geochemical, elemental and sedimentological data plotted against time (Figs. 8, 9). Based on these considerations, five different periods have been distinguished for this subtropical lake characterizing its Holocene environmental history.

(1) Early Holocene (10,400-7800 cal. BP) – dominance of fluvial sedimentation: This period is composed of LZs A1 and C and characterized by cluster 2 with increased values of Fe, K and Ti (Fig. 9) in a medium silt matrix. This type of sediment is introduced by suspension fallout during flooding of Rio Guabiroba. Moreover, the elemental composition excludes the Furnas Formation as a source of these deposits, because Fe and K are unknown from the sandstone of the Furnas Formation making river influence the only possible source. In terms of organic sediment components, the onset at 10,400 cal. BP reflects rather low values for TOC and BSi (Fig. 8). While TOC remains at such a low level throughout this period, diatom productivity (BSi) increases rapidly and reaches two distinct maxima at 8300 and 8000 cal. BP, both with microscopically detectable high numbers of planktonic diatoms. This increased diatom productivity might be fostered by the relatively high amounts of K and Si together with other micronutrients essential for diatom growths introduced through fluvial discharge, while N remains rather low (Fig. 8) leaving non-siliceous algae at low numbers. In general, the lacustrine system of the Early Holocene is characterized by an increasing nutrient level, while the source of OM is dominantly lacustrine (C/N ratio: 10-15).

Rio Guabiroba flows on its flood plain with a very low gradient. This is indicated by the high degree of meandering along the river course (Fig. 1), which leads to the deposition of silt and sand in the river bed. During flooding, silt and fine sand are deposited on the river banks forming a levee and finer grains cover the flood plain. Lagoa Dourada is situated on this flood plain and has a short-cut connecting the river with the lake. As flooding through this outflow channel occurs against the local gradient, flow velocity is expected to be low and only silt and clay can be transported and eventually deposited in the lake basin as suspension fallout. This process is supported by observations during coring, when low lake-water transparency due to high suspension loads occurred during a flood event changing to high lake-water transparency virtually hours after the flood event has ended.

Another aspect to be mentioned is the availability of fine-grained material for river transport and deposition. Initially such material needs to be eroded, but erosion only occurs if the soil is not well protected by the vegetation. Moreover, the type of rainfall increases the susceptibility to erosional processes: episodic precipitation during a drier climate results in higher erosion rates compared to more evenly distributed precipitation during a wetter climate. This would exclude forest as vegetation type for the Early Holocene as it protects from soil erosion. Thus, decreasing silt deposition during the subsequent early Middle Holocene transitional period could be explained by forest expansion as the consequence of higher rainfall reducing soil erosional processes. Another possible explanation could be that levees have been created in the course of several millennia with flooding protecting the flood plain more efficiently from flooding.

The final centuries of the Early Holocene (8300-7800 cal. BP) are characterized by an all-time maximum in planktonic diatom development (Fig. 8), a marked decrease in Ti as well as a distinct increase in K (Fig. 9). Together, this could be explained by increased precipitation, which would correspond to less soil erosion due to a denser vegetation cover (Ti), a higher degree of chemical weathering with related leaching of K and a deeper lake with more nutrients beneficial for planktonic diatom development (Fig. 9). This wet period may represent the 8.2 ka event, which is characterized – according to model simulations – by more rainfall in South Brazil as a result of North Atlantic cooling and monsoon enhancement across Brazil (Morrill et al., 2013).

(2) Early Middle Holocene transition (7800-6200 cal. BP) – from dominance of fluvial influence to autochthonous lacustrine deposition: This combination of LZs A2 and D1 is a two-partite transitional period belonging to clusters 2 and 4. On the one hand, BSi drops from 20 to 3 % right at the beginning of this period and remains constantly low further on. On the other hand, TOC triples to values up to 15 %. This development goes along with an increase of the C/N ratio from 12 to 30, a change starting with a delay of 400 years, which indicates a higher influence of allochthonous OM. This process parallels an increase in mean grainsize from 20 µm (middle silt) to 70 µm (fine sand) and is completed by 7000 cal. BP. Since then and until the end of the early Middle Holocene at 6200 cal.

BP, C/N and grainsize remain at their high levels. A component related to OM that additionally comes into play during the latter part of this period is S (Fig. 9). This element is low during the first part of this transition and increases markedly after 7400 cal. BP – a change that goes along with an increase in Fe. Formation of pyrite explains this process pointing to anoxic conditions at the lake floor and being responsible for the color change to darker hues with the onset of LZ D1. Finally, elements of the minerogenic sediment component relating to the river catchment area as source (K, Ti) loose importance towards the end of this transition period (Fig. 9).

There are two possible options explaining the transition from silt-dominated sediments poor in OM to an increasing sand-dominance with more allochthonous OM. The general process behind this development is less influence of river flooding. Simultaneously, increasing influence of organic lacustrine productivity and/or runoff from the immediate catchment area of Lagoa Dourada with influx of allochthonous OM such as leaves and twigs responded in higher C/N ratios. Buildup of levees preventing the floodplain from flooding could be regarded as an explanation. However, as the outflow channel from the lake always keeps an opening in the levee, this option seems less likely. Instead, it is more likely that higher and more evenly distributed precipitation increased the density of vegetation, which on the one hand protects soils in the wider catchment area of Rio Guabiroba from erosion and thus reduces availability and river transport of fine-grained minerogenic matter. On the other hand, less suspension transport of the river frees fluvial energy activating increased incision into the river bed and reducing the likelihood of flooding. As the second mechanism can be explained favorably by increased rainfall, we assume this process to be the most likely case explaining the change in depositional processes.

More precipitation is also regarded as the reason for (1) higher activity of the karst hydrological system responsible for introducing sand into the lake; (2) intensified chemical weathering and thus increased pedogenesis in combination with denser vegetation making available more nutrients such as N and P (cf., Fig. 3 for N). Moreover, the decrease in diatom abundance suggests other algae, such as blue-green algae (cyanobacteria), as being responsible for a fueled lacustrine productivity leading to anoxia in the lake with the formation of pyrite; and (3) an increased density of vegetation, which explains the higher contribution of allochthonous and lignin-rich OM responsible for increasing C/N ratios. The underlying change from a drier to a wetter landscape with adapting vegetation might be considered the reason for this transition indicated by highest C/N ratios and sand influx. It is interesting to note that this transitional period is framed by two (LZs B2 and E1) and includes a third (LZ B3) out of five sand horizons, which make up almost 87 % of the thickness of all sand layers confirming still unstable environmental conditions in the catchment area.

(3) Late Middle Holocene (6200-3800 cal. BP) – stabilization of lacustrine deposition: During the late Middle Holocene (LZ D2) the ecosystem stabilized with increasingly organic sediment deposition. Although BSi remains at its low level, TOC continues to rise to 20 % until 4600 cal. BP, when a distinct drop to 10 % occurs until 3800 cal. BP. The only other parameter marking this change is grainsize, which coarsens towards a mean of >100 µm. Thus, the drop in TOC likely is a result of dilution by additional quartz grains. However, the C/N ratio is decreasing, which excludes intensified surface runoff and suggests a very stable catchment system with increased influx of sand via karstic springs. This is supported by continuing high levels of the element S indicating anoxia as the result of increased organic lacustrine productivity probably dominated by blue-green algae.
Altogether, the lacustrine system further stabilized during this period as well as the catchment area, from where less terrestrial organic remains enter the lake and thus cause the C/N ratio to decrease. However, prior to the onset of the Late Holocene at 4600 cal. BP, an increased activity of the karst hydrological system indicates wetter environmental conditions not only causing an increase in grain size but also the formation of the youngest sand layer at the termination of this period (3800 cal. BP).

(4) Late Holocene (3800-600/150[1] cal. BP) – mature lacustrine deposition: Until 600/150[1] cal. BP the lake system matures in the course of LZ D3. OM steadily increases to a maximum of >25 % TOC and also BSi doubles to 5 %. At the same time, the C/N ratio decreases indicating a more prominent contribution of autochthonous lacustrine OM. This is supported by S remaining at the same high level as during the Middle Holocene and documenting the presence of anoxia at the lake bottom. Grainsize diminishes from a mean of 50 to 30 µm as well as siliciclastic elements (K, Ti) decrease, documenting that minerogenic components are at their minimum. Altogether, the lake develops towards more eutrophic conditions with two TOC maxima at 1750 and 1000 cal. BP.

The final ca. 400 years of this period are characterized by distinctly dropping values for Ti and K. Decreasing values can be explained by denser vegetation inhibiting soil erosion, which would argue for higher precipitation as the responsible factor, i.e. a strengthening of the SAMS, comparable to the observation made for the 8.2 ka event. Due to more humid conditions with distinctly reduced export of the erosion-related elements Ti and K (lowest value of the entire record for Ti), these four centuries (550[1]-150[1] cal. BP or AD 1400-1800) are suggested as corresponding with the LIA.

(5) Human impact (600/150[1] cal. BP – present day) – returning dominance of fluvial sedimentation during the last centuries: A drastic sedimentological change occurs after the preceding mature period within LZs F and G. Not only TOC, BSi, C/N ratio and grainsize decrease markedly in LZ F (Fig. 8), also all elemental data (Fig. 9) respond accordingly: S and Si drop to lower values while Fe, K and Ti increase. S covaries with all organic productivity indicating proxies, which either points to a drop in organic productivity or to dilution by minerogenic matter. The latter seems to be the more likely explanation here because Fe is no longer correlating with S but with K and Ti instead. This indicates an increased presence of siliciclastic matter, which is supported by a change in color and higher K and Ti levels. The simultaneous drop in Si as well as the presence of Fe suggest that during this period the lake again received suspended sediment loads from Rio Guabiroba, as Fe and K are no constituents of sandstones from the Furnas Formation. Similarly, fine silt observed as the mean grainsize (6 µm) with highest contributions of clay (up to 33 %) is neither a component of the Furnas sandstone.

If this sediment is the result of re-activated flooding of the river (cluster 3) then the question arises, which processes caused these deposits and shape them so markedly different from Early Holocene suspension load (cluster 2). The most convincing explanation includes human activity related to land-use change. During wetter environmental conditions since the Middle Holocene, the vegetation became denser. Moreover, chemical weathering and pedogenesis altered the soils causing enrichment in Fe, depletion in K and formation of the clay mineral kaolinite. These soils were stabilized by the vegetation until European farmers claimed the land. While the vegetation protects soils from erosion even under high rainfall conditions, land clearance, often with the help of fire, immediately triggered erosional processes (cf., Zolitschka, 1998). As the soil-protecting canopy and the stabilizing root system are removed, less water is stored in vegetation and in soil OM increasing surface runoff and causing soil erosion. Relocated downslope, the river picks up the eroded material and transports it towards Lagoa Dourada. This high sediment freight of Rio Guabiroba gave rise to a high amount of deposition in the river bed, thus decreasing its cross section and at the same time increasing the probability of flooding, which is regarded as the reason for deposition of LZ F.

However, this plausible interpretation of LZ F contradicts with the age-depth model suggesting 600 cal. BP for the onset of human activities, i.e. AD 1350. This date opposes historical data of first European settlements in South Brazil documented for around AD 1750 (Freitas, 2011) with still marginal influences on the landscape. Only decades later, land-use change accelerated between AD 1800 and 1850 (Freitas, 2011). Altogether, this challenges the age-depth model for the last millennium with only one radiocarbon date at 850 cal. BP (Tab. 1, Fig. 7). We, therefore, suggest to

[1] See later discussion for explaining the younger date.

add the historical date of AD 1800 ±50 for the onset of agricultural activities in the hydrological catchment (Fig. S6).

A different explanation of clastic LZ F is possible if the age-depth model is assumed to be correct (Fig. 7). For the time from 600-200 cal. BP (AD 1350-1750) natural climatic variability, such as the Little Ice Age (LIA), might be considered as a reason. Only few paleorecords provide evidences of the LIA for South Brazil. However, this is most likely a matter of temporal resolution being less adequate for detecting this climatic fluctuation (cf., Bernal et al., 2016). However, assuming the LIA as the reason for LZ F, causative processes would not be supported by the sediment record of Lagoa Dourada. The impact of the LIA on climatic conditions that can be expected for S Brazil is increased precipitation (Bernal et al., 2016; Novello et al., 2021) leading to denser vegetation with less soil erosion. This is a process actually described for the centuries immediately prior to LZ F. Thus, we refuse the option of considering the LIA as responsible for an increase in minerogenic deposition during LZ F and find further support for a modification of the chronology (Fig. S6).

This interpretation in combination with the modified age-depth model is also supported by the topmost lithozone (LZ G), which is characterized by a return to highly organic deposits (Fig. 8) around AD 1950 (Fig. S6). This corresponds with the establishment of the Vila Velha State Park in AD 1953. In combination with reforestation with pine and eucalypt during the following decade, soil erosion was immediately reduced. A return to highly organic sediments comparable to those prior to AD 800 was the result, except for two elements: N (Fig. 3) and K (Fig. 5, 9). Both elements increase considerably towards the top of the record, a process explained by the extensive use of fertilizers in the catchment area since the 1950ies.

Discussion

<u>Chronological considerations</u>: Evidences in support of the Early Holocene start of our chronology exist from various sources. Although uncalibrated radiocarbon ages date the base for LD17-91 to 11,170 BP (Melo et al., 2003; Moro et al., 2004) and for LD17-17 to 13,850 BP, these Late Pleistocene ages are influenced by reservoir effects and are not providing a Lateglacial age for the basal sediments from Lagoa Dourada. This is confirmed by pollen and speleothem data. Palynological investigations at Serra dos Orgaos (22.5 °S) describe a warm and wet Younger Dryas (YD) chronozone (Behling and Safford, 2010). Similar climatic conditions are reconstructed with pollen from Serra do Tabuleiro at 28 °S (Behling and Oliveira, 2017). Additionally, the reconstruction of precipitation using stable isotopes of a speleothem from Botuverá Cave at 27 °S (Cruz et al., 2005) also characterizes the YD as wet comparable to the Late Holocene. There is no evidence for such a wet period with forest expansion at the base of our record (Piraquive Bermúdez, 2020). Thus, we have further evidence that the obtained Lateglacial ages are artefacts and the record from Lagoa Dourada starts during the Early Holocene.

At the upper end of the stratigraphy, pollen-based evidence of deforestation exists from tropical Lago do Pires (18 °S) dated to 140 BP (Behling, 1995), which corresponds to AD 1840 after calibration. At Cambara do Sul (29 °S) human activities started after AD 1780, first with cattle breeding followed by logging. Since AD 1820, settlements were established with accompanying agriculture (Behling et al., 2004). Also at Serra da Bocaina (23 °S) permanent European communities were established after AD 1750 (Portes et al., 2018). Furthermore, historic evidence for the introduction of neophytes (eucalypt and pine trees) to South Brazil dates back to AD 1904, when timber barons established first tests with these fast-growing species (Ayling and Martins, 1981). However, commercial eucalypt plantations near Lagoa Dourada did not occur before the mid-1960ies (Ayling and Martins, 1981). They are reported for Vila Velha State Park for AD 1964 (Government of the State of Parana). Thus, we are confident that LZ G covers only the last ~70 years. The reason for this discrepancy of historical data with the radiocarbon-based age-depth model is the lack of ^{14}C ages for the last millennium, where distinct changes in sedimentation rate additionally modify the record (Fig. S6).

Comparison with previously published data from Lagoa Dourada: Sediments from Lagoa Dourada (LD91) have been cored for the first time 30 years ago (Melo et al., 2003; Moro et al., 2004). However, this record is severely hampered by (1) very general sediment descriptions differing between Melo et al. (2003) and Moro et al. (2004); (2) many of the data are available with only low spatial resolution (1 or 2 analyses/m); and (3) the chronology is based on two radiocarbon dates providing ages of 11,170 ±110 BP and 8720 ±150 BP from 11,9 m and 10.6 m, respectively. With these dates, a Lateglacial age has been proposed for the basal sediments at 12.2 m. As a result of our study, these ages should be considered cautiously and not without considering a reservoir correction. Despite of these limitations, Melo et al. (2003) provide mineralogical data based on XRD analyses, which document the presence of quartz, kaolinite, illite, pyrite and gypsum. The latter is an artefact and produced after core splitting when pyrite (FeS) oxidized and recrystallized as gypsum ($CaSO_4$). As total carbon percentages of the old record are erroneously low (<0.83 %), the presence of pyrite together with gypsum is interpreted as an indicator of dry (semi-arid) climate conditions prior to 8720 BP and for a period between 5000 and 3000 BP (Melo et al., 2003). Furthermore, it is argued that the sand horizons are related to semi-arid conditions, when river runoff and thus flooding events did not occur while karstic springs provided water with quartz grains. While our study does not support these assumptions, the detection of a planktonic diatom maximum at 11.8 m by Moro et al. (2004) agrees with LZ C with its high BSi values and the microscopic detection of planktonic diatoms. Moreover, Moro et al. (2004) confirm the largest concentration of K for a depth of 20 cm, which is related to NPK fertilizers applied in the catchment area.

Comparison with pollen data from S and SE Brazil: Most paleoenvironmental data from S and SE Brazil is from palynological investigations. Here we compare our investigation with pollen records spanning a latitudinal range from 18 to 28 °S.

The pollen record from Serra do Tabuleiro (28 °S) provides a nicely dated and densely analyzed Early Holocene record (Behling and Oliveira, 2017). After the warm and wet second half of the YD, Campos vegetation (grassland) with a warm and dry climate dominated the Early Holocene until 8000 cal. BP. Compiling eleven pollen records covering the latitudes between 15 and 35 °S, Ledru et al. (1998) document warm and dry Early Holocene climatic conditions for the time period 11,400-7700 cal. BP. In a comparable synthesis, Behling (2002) uses 14 pollen records between 18 and 28 °S and suggests ~6300 cal. BP as the end of warm and dry Early Holocene conditions. This data supports our interpretation of Lagoa Dourada environmental conditions, where grassland vegetation under dry and warm climate conditions is proposed to explain erosion of fine-grained material in the catchment area via slope-wash (no trees that protect against soil erosion), river transport and flooding until 7800 cal. BP (Fig. 8). This is also supported by data from NE Brazil, where the Middle Holocene shift from forest to grassland vegetation (Caatinga), i.e. from wet to dry conditions, caused an increase in soil-erosion rates due to less dense vegetation exposing soils to erosion during precipitation events (Jaqueto et al., 2016; Utida et al., 2020). This process not only caused intense colluvial deposition but also the formation of the highest fluvial terraces in the drainage systems of South Brazilian rivers dated to 11,400-9500 cal. BP (Suguio et al., 1989).

After a warm and dry onset of the Holocene, precipitation started to increase, causing a change from Campos to the development of forest at Serra do Tabuleiro (Behling and Oliveira, 2017). Increased moisture advection from the Amazon Basin with a weakening of polar advection results in an expansion of forests in South Brazil dated to 7700-4390 cal. BP (Ledru et al., 1998). This process is not consistent in timing across S and SE Brazil (cf., Behling, 2002), a fact that may be due to the large latitudinal extension (1300 km) of available data, differences in elevation between coastal plains and the mountainous hinterland, chronological uncertainties but may also be related to a time-transgressive spatial evolution of climatic conditions. Higher rainfall with the expansion of forest is noted by other pollen records for a time period from 8900 until 5700 cal. BP (Behling, 1995, 2003; Behling and Oliveira, 2017; Behling and Safford, 2010; Enters et al., 2010; Rodrigues-Filho et al., 2002). This change from grassland to forest reduced hillslope denudation to a minimum and increased chemical weathering and pedogenesis with leaching of nutrients as documented by an increased lacustrine productivity at Lago Aleixo (Enters et al., 2010). This also transformed lacustrine sedimentological processes at Lagoa Dourada and at Lago Silvana at 19,5 °S from silt-rich suspension fallout to Fe-rich organic sediments (Rodrigues-Filho et al., 2002).

Organic deposition continued until the last millennium when a few sites document a climatic fluctuation related to the LIA with warm and wetter climatic conditions. These have been detected for AD 1520-1780 at Cambara do Sul (Behling et al., 2004) and since AD 1390 at Lagoa Nova (Behling, 2003). For Lagoa Dourada only a weak signal with less siliciclastic matter (K and Ti in Fig. 9) is detected and possibly related to a LIA age of AD 1350-1800 according to the modified chronology (Fig. S6).

In a next step, human activities changed the ecosystems. Since the late 18th century, European settlers started to use the area for farming (Behling and Oliveira, 2017; Portes et al., 2018). Agricultural activities gave rise to increased soil erosion, as documented for Lagoa Dourada and less prominent for Lago Aleixo (Enters et al., 2010). In both cases, organic sediments were replaced by minerogenic sediments.

Comparison with regional speleothem data: Speleothems currently provide the best dated and most significant climatic parameters for the reconstruction of precipitation in NE and SE Brazil (Baker and Fritz, 2015). In a distance of only 240 km SSE from Lagoa Dourada, speleothems from Caverna Botuverá (27 °S) provide high-resolution stable isotope data with a precise U/Th-based chronology dating back to 116 ka (Cruz et al., 2005). The obtained oxygen isotope record (Fig. 10a) varies with the source of precipitation and thus is interpreted as a proxy for atmospheric circulation and convective intensity, both closely related to the SAMS controlling hydroclimatic conditions. Summer convection over the Amazon Basin and associated monsoonal precipitation in South Brazil has a more negative oxygen isotope signature compared to winter rain related to incursions of mid-latitudinal storm tracks from the Atlantic Ocean (Cruz et al., 2005). These conditions are nicely summarized by Wang et al. (2007): “Low (high) Bouverá speleothem $\delta^{18}O$ indicates intensified (weakened) SASM activity, more (less) Amazon moisture contribution and higher (lower) rainfall in South Brazil.” Thus, the isotopic record from Caverna Botuverá is linked to variability in precipitation caused by insolation-controlled fluctuations of the SAMS and provides one of the most robust climate reconstructions for South America. While the early studies of Caverna Botuverá focus on orbital to millennial timescales (Cruz et al., 2005; Wang et al., 2007), follow-up investigations obtained a much higher temporal resolution for the Holocene detecting decadal to centennial climatic variability (Bernal et al., 2016; Novello et al., 2021), data which also were used for inter-hemispheric correlation of climate modes (Deininger et al., 2020). The high-resolution $\delta^{18}O$ data are supported by even higher resolving trace-element data (Mg, Ca, Sr, Ba). Especially the Sr/Ca ratio correlates highly with $\delta^{18}O$ (Fig. 10b, c) and is applied as a proxy that characterizes SAMS intensity and detects the effect of Holocene climate anomalies on regional hydroclimatic conditions while closely following summer insolation at 30 °S (Bernal et al., 2016). These data document a suppressed SAMS intensity during the Early Holocene and an increase starting around 7000 cal. BP. Due to the well-dated and high-resolution record, also centennial climatic events of the Holocene have been detected: the 8.2 ka event and the LIA for the time interval AD 1400-1850 (Bernal et al., 2016) – both characterized by a wetter hydroclimate. A wet LIA (AD 1600-1850) with stronger SAMS is also documented by a compilation of speleothem $\delta^{13}C$ data from 25 caves in tropical and subtropical South America (Novello et al., 2021). All speleothem data about the regional hydroclimate are in line with our interpretation of the high-resolution record from Lagoa Dourada, underline the environmental changes observed and provide the best possible precipitation signal, which solidifies the reconstructed surface processes that lead to the formation of the studied sediment sequence.

The 8.2 ka event is characterized here by increased BSi related to a maximum in planktonic diatom development (Fig. 8), a marked decrease in Ti and an increase in K (Fig. 9). These two centuries match with the increased precipitation, which corresponds to less soil erosion due to denser vegetation (Ti), a higher degree of chemical weathering with related leaching of K and a deeper lake with more nutrients beneficial for the development of planktonic diatoms (Fig. 8).

Conclusions

Thirty years after first investigations of sediment from Lagoa Dourada (South Brazil), our re-visit of the site provides a wealth of information shedding new light on environmental responses triggered by dominating climatic control mechanisms related to the intensity variations of the South American Monsoon System (SAMS). We recovered two overlapping sediment profiles that extend the previous record (Melo et al., 2003; Moro et al., 2004) more than 2 m into the past. Time control is obtained by applying sophisticated age-depth modelling after combining AMS radiocarbon dates on terrestrial macrofossils with reservoir-corrected ages of bulk OM. Based on this chronology, XRF core-scanning data together with geochemical and sedimentological studies provide high-resolution insights into responses of lacustrine and geomorphological systems to climatic variability and anthropogenic impacts. Altogether, this allows investigating a detailed regional hydroclimatic history and provides unequivocal linkages to other regional and high-resolution studies, namely the speleothem records from Caverna Botuverá (Bernal et al., 2016; Novello et al., 2021).

Based on statistical analyses of the high-resolution dataset from Lagoa Dourada, four different sediment sources were characterized geochemically and relate to lacustrine organic productivity, underground karst runoff, river flooding and cultural soil erosion. Thus, our comprehensive and well-dated multiproxy dataset provides a handle on process-related developments in the lake and its catchment area and allows insights into physical landscape changes as well as into geomorphological and lacustrine processes – all reflecting environmental responses to hydroclimatic variability during the Holocene and to human activities during the last few centuries. As such, this new record from Lagoa Dourada fills a knowledge gap with regard to hydroclimatic variability and its impact on environmental systems for South Brazil and beyond. Moreover, these sediments provide an essential contribution to understand how precipitation changes influenced the resilience of ecosystems and their responses to global climate change, which is important background information to better constrain model projections of future precipitation and their impacts on environmental change.

Our high-resolution data documents dominating flooding through Rio Guabiroba with suspension fallout of minerogenic particles transferred to the lake via fluvial activity during the Early Holocene. Between 7800 and 6200 cal. BP, a transition to highly organic lacustrine deposits is observed, when fluvial influences were replaced by increasingly organic deposition. This is due to decreasing availability of minerogenic particles from hillslope denudation and river transport as a result of intensified pedogenesis under developing forests. Furthermore, this transition period is characterized by sand horizons, which link to more runoff through the karst hydrological system – a process less well understood but also linked to increased precipitation. Once established, autochthonous lacustrine processes dominate sediment formation for the remaining Holocene, except for the topmost centuries. Based on a modified age-depth model for the last millennium, between AD 1800 and 1950 European settlers caused severe soil erosion as a result of land-use change. For the topmost and youngest seven decades, organic deposition reconvenes with evidences of increased eutrophication documented by high values for nitrogen and potassium acting as nutrients for lake biota.

The climatic development from a warm and dry Early Holocene to a warm and wet Middle and Late Holocene is in response to strengthening of the SAMS. In addition to this general trend, the sediment record from Lagoa Dourada most likely documents imprints of the two most prominent Holocene climatic events: the 8.2 ka event and the Little Ice Age. For Lagoa Dourada, both reflect a several century-long increase in rainfall with complex responses of the environmental system. This result favorably agrees with the climatic signal preserved by the speleothem record from Caverna Botuverá (Bernal et al., 2016).

Future tasks to exploit this sediment record even further should (1) improve the chronology of the last millennium with radiometric dating (^{14}C, ^{210}Pb), (2) link sedimentological and geochemical results with paleobiological data such as pollen (Piraquive Bermúdez, 2020) and diatoms (Moro et al., 2004) to improve our understanding of interactions between regional vegetation and the geomorphological system in response to climate change and (3) extend investigations to stable isotopes of OM to better characterize and understand the Middle Holocene transition from C4 to C3 plants. Another and completely different challenge would be related to coring longer sediment records from Lagoa Dourada with the ultimate goal to penetrate the Pleistocene and to discover imprints of environmental changes linked to the Younger Dryas and the Antarctic Cold Reversal.

Data Availability

The multiproxy dataset of the lacustrine sediment record from Lagoa Dourada is accessible via the PANGAEA data archiving and publication system at https://doi.pangaea.de/10.1594/PANGAEA.xxxxxx. [The correct link will be provided during revisions.]

Supplemental Material

Supplementary figures and tables to this article are available online.

Acknowledgements

We are grateful to Vivian Luciana Jeske-Pieruschka (Universidade Federal do Ceará, Fortaleza, Brazil) for assistance in the field and organizing permits for the Vila Velha State Park at Instituto Ambiental do Paraná (number: 55.16). Support for sample preparation and analyses in the GEOPOLAR lab (University of Bremen) was provided by Carsten Smidt, Sabine Stahl and Rafael Stiens. Thanks also go to Hermann Behling (University of Göttingen) for support with field work and for critical comments on the draft as well as to Lujan Garcia (University of Bremen) for improving an earlier version of this manuscript. This research was funded by the Deutsche Forschungsgemeinschaft (DFG, German Research Foundation) as project GI 732/8-1.

References

Abdi, H., Williams, L.J., 2010. Principal Component Analysis. John Wiley & Sons, Ltd. https://doi.org/10.1002/wics.101

Aitchison, J., 1982. The statistical analysis of compositional data. Journal of the Royal Statistical Society. Series B: Statistical Methodology 44, 139–177.

Ayling, R.D., Martins, P.J., 1981. The growing of eucalypts on short rotation in Brazil. The Forestry Chronicle February 1981, 9-16.

Baker, P.A., Fritz, S.C., 2015. Nature and causes of Quaternary climate variation of tropical South America. Quaternary Sci Rev 124, 31-47. http://dx.doi.org/10.1016/j.quascirev.2015.06.011

Behling, H., 1995. A high resolution Holocene pollen record from Lago do Pires, SE Brazil: vegetation, climate and fire history. Journal of Paleolimnology 14, 253-268.

Behling, H., 2002. South and southeast Brazilian grasslands during Late Quaternary times: a synthesis. Palaeogeogr Palaeocl 177, 19-27. http://dx.doi.org/10.1016/S0031-0182(01)00349-2

Behling, H., 2003. Late glacial and Holocene vegetation, climate and fire history inferred from Lagoa Nova in the southeastern Brazilian lowland. Vegetation History and Archaeobotany 12, 263-270. http://dx.doi.org/10.1007/s00334-003-0020-9

Behling, H., Oliveira, M.A.T.d., 2017. Evidence of a late glacial warming event and early Holocene cooling in the southern Brazilian coastal highlands. Quaternary Research 89, 90-102. http://dx.doi.org/10.1017/qua.2017.87

Behling, H., Pillar, V.D., Orlóci, L., Bauermann, S.G., 2004. Late Quaternary Araucaria forest, grassland (Campos), fire and climate dynamics, studied by high-resolution pollen, charcoal and multivariate analysis of the Cambará do Sul core in southern Brazil. Palaeogeography, Palaeoclimatology, Palaeoecology 203, 277-297. http://dx.doi.org/10.1016/s0031-0182(03)00687-4

Behling, H., Safford, H.D., 2009. Late-glacial and Holocene vegetation, climate and fire dynamics in the Serra dos Órgãos, Rio de Janeiro State, southeastern Brazil. Global Change Biology 16, 1661-1671. http://dx.doi.org/10.1111/j.1365-2486.2009.02029.x

Behling, H., Safford, H.D., 2010. Late-glacial and Holocene vegetation, climate and fire dynamics in the Serra dos Órgãos, Rio de Janeiro State, southeastern Brazil. Global Change Biology 16, 1661-1671. http://dx.doi.org/10.1111/j.1365-2486.2009.02029.x

Bernal, J.P., Cruz, F.W., Stríkis, N.M., Wang, X., Deininger, M., Catunda, M.C.A., Ortega-Obregón, C., Cheng, H., Edwards, R.L., Auler, A.S., 2016. High-resolution Holocene South American monsoon history recorded by a speleothem from Botuverá Cave, Brazil. Earth and Planetary Science Letters 450, 186-196. http://dx.doi.org/10.1016/j.epsl.2016.06.008

Blaauw, M., Christen, J.A., Aquino Lopez, M.A., 2021. rbacon: Age-Depth Modelling using Bayesian Statistics, R package version 2.5.1. ed.

Blott, S.J., Pye, K., 2001. GRADISTAT: a grain size distribution and statistics package for the analysis of unconsolidated sediments. Earth Surface Processes and Landforms 26, 1237-1248. http://dx.doi.org/10.1002/esp.261

Bronk Ramsey, C., 2009. Bayesian analysis of radiocarbon dates. Radiocarbon 51, 337–360.

Carnaval, A.C., Hickerson, M.J., Haddad, C.F.B., Rodrigues, M.T., Moritz, C., 2009. Stability Predicts Genetic Diversity in the Brazilian Atlantic Forest Hotspot. Science 323, 785-789. http://dx.doi.org/10.1126/science.1166955

Croudace, I.W., Löwemark, L., Tjallingii, R., Zolitschka, B., 2019. Current perspectives on the capabilities of high resolution XRF core scanners. Quatern Int 514, 5-15. http://dx.doi.org/10.1016/j.quaint.2019.04.002

Croudace, I.W., Rindby, A., Rothwell, R.G., 2006. ITRAX: description and evaluation of a new multi-function X-ray core scanner, in: Rothwell, R.G. (Ed.), New techniques in sediment core analysis. The Geological Society of London Special Publications, London, pp. 51-63.

Croudace, I.W., Rothwell, R.G., 2015. Future Developments and Innovations in High-Resolution Core Scanning. Dev Paleoenviron Res 17, 627-647. http://dx.doi.org/10.1007/978-94-017-9849-5_27

Cruz, F.W., Burns, S.J., Jercinovic, M., Karmann, I., Sharp, W.D., Vuille, M., 2007. Evidence of rainfall variations in Southern Brazil from trace element ratios (Mg/Ca and Sr/Ca) in a Late Pleistocene stalagmite. Geochimica et Cosmochimica Acta 71, 2250-2263. http://dx.doi.org/10.1016/j.gca.2007.02.005

Cruz, F.W., Burns, S.J., Karmann, I., Sharp, W.D., Vuille, M., Cardoso, A.O., Ferrari, J.A., Silva Dias, P.L., Viana Jr, O., 2005. Insolation-driven changes in atmospheric circulation over the past 116,000 years in subtropical Brazil. Nature 434, 63-66. http://dx.doi.org/10.1029/

Dearing, J., 1994. Environmental magnetic susceptibility: using the Bartington MS2 system. Chi Publishing, Keniloworth.

Deininger, M., McDermott, F., Cruz, F.W., Bernal, J.P., Mudelsee, M., Vonhof, H., Millo, C., Spotl, C., Treble, P.C., Pickering, R., Scholz, D., 2020. Inter-hemispheric synchroneity of Holocene precipitation anomalies controlled by Earth's latitudinal insolation gradients. Nat Commun 11, 5447. http://dx.doi.org/10.1038/s41467-020-19021-3

Deininger, M., Ward, B.M., Novello, V.F., Cruz, F.W., 2019. Late Quaternary Variations in the South American Monsoon System as Inferred by Speleothems—New Perspectives using the SISAL Database. Quaternary 2. http://dx.doi.org/10.3390/quat2010006

Enters, D., Behling, H., Mayr, C., Dupont, L., Zolitschka, B., 2010. Holocene environmental dynamics of south-eastern Brazil recorded in laminated sediments of Lago Aleixo. Journal of Paleolimnology 44, 265-277. http://dx.doi.org/10.1007/s10933-009-9402-z

Folk, R.L., Ward, W.C., 1957. Brazos river bar: a study in the significance of grain size parameters. Journal of Sedimentary Petrology 27, 3-26.

Freitas, F., 2011. Land Use and Deforestation in Southeastern Brazil — 1753-1840, pp. https://fredericofreitas.org/2011/2011/2018/land-use-and-deforestation-in-southeastern-brazil-1753-1840/#f2011.

Harris, C.R., Millman, K.J., van der Walt, S.J., Gommers, R., Virtanen, P., Cournapeau, D., Wieser, E., Taylor, J., Berg, S., Smith, N.J., Kern, R., Picus, M., Hoyer, S., van Kerkwijk, M.H., Brett, M., Haldane, A., del Río, J.F., Wiebe, M., Peterson, P., Gérard-Marchant, P., Sheppard, K., Reddy, T., Weckesser, W., Abbasi, H., Gohlke, C., Oliphant, T.E., 2020. Array programming with NumPy. Nature 585, 357-362. http://dx.doi.org/10.1038/s41586-020-2649-2

Hogg, A., Heaton, T., Hua, Q., Palmer, J., Turney, C., Southon, J., Bayliss, A., Blackwe Boswijk, G., Bronk Ramsey, C., Pearson, C., Petchey, F., Reimer, P., Reimer, R., Wacker, L., 2020. SHCal20 Southern Hemisphere calibration, 0-55,000 years cal BP. Radiocarbon 62. http://dx.doi.org/10.1017/RDC.2020.59

Hunter, J.D., 2007. Matplotlib: A 2D Graphics Environment. Computing in Science and Engineering 9, 99–104.

Jaqueto, P., Trindade, R.I.F., Hartmann, G.A., Novello, V.F., Cruz, F.W., Karmann, I., Strauss, B.E., Feinberg, J.M., 2016. Linking speleothem and soil magnetism in the Pau d'Alho cave (central South America). Journal of Geophysical Research: Solid Earth 121. http://dx.doi.org/doi:10.1002/2016JB013541

Ledru, M.-P., Mourguiart, P., Riccomini, C., 2009. Related changes in biodiversity, insolation and climate in the Atlantic rainforest since the last interglacial. Palaeogeography, Palaeoclimatology, Palaeoecology 271, 140-152. http://dx.doi.org/10.1016/j.palaeo.2008.10.008

Ledru, M.-P., Salgado-Labouriau, M.L., Lorscheitter, M.L., 1998. Vegetation dynamics in southern and central Brazil during the last 10,000 yr B.P. Review of Palaeobotany and Palynology 99, 131-142.

Liu, X., Colman, S.M., Brown, E.T., Minor, E.C., Li, H., 2013. Estimation of carbonate, total organic carbon, and biogenic silica content by FTIR and XRF techniques in lacustrine sediments. Journal of Paleolimnology 50, 387-398. http://dx.doi.org/10.1007/s10933-013-9733-7

Lorscheitter, M.L., Takeda, I.J.M., 1995. Reconstituição paleoambiental da região dos Campos Gerais, Paraná, através da palinologia de sedimentos da Lagoa Dourada, V Congresso da Associação

Brasileira de Estudos do Quaternário, XI Simpósio de Sedimentologia Costeira, . Anais. Niterói, ABEQUA, 18-21, Niterói, RJ, pp. 18-21.

Löwemark, L., Bloemsma, M., Croudace, I., Daly, J.S., Edwards, R.J., Francus, P., Galloway, J.M., Gregory, B.R.B., Steven Huang, J.-J., Jones, A.F., Kylander, M., Löwemark, L., Luo, Y., Maclachlan, S., Ohlendorf, C., Patterson, R.T., Pearce, C., Profe, J., Reinhardt, E.G., Stranne, C., Tjallingii, R., Turner, J.N., 2019. Practical guidelines and recent advances in the Itrax XRF core-scanning procedure. Quatern Int 514, 16-29. http://dx.doi.org/10.1016/j.quaint.2018.10.044

Martin-Puertas, C., Tjallingii, R., Bloemsma, M., Brauer, A., 2017. Varved sediment responses to early Holocene climate and environmental changes in Lake Meerfelder Maar (Germany) obtained from multivariate analyses of micro X-ray fluorescence core scanning data. Journal of Quaternary Science 32, 427-436. http://dx.doi.org/10.1002/jqs.2935

McInnes, L., Healy, J., Astels, S., 2017. Hdbscan: Hierarchical Density Based Clustering. The Journal of Open Source Software 2, 205. http://dx.doi.org/http://joss.theoj.org/papers/10.21105/joss.00205

Melo, M.S., Giannini, P.C.F., Pessenda, L.C.R., Neto Brandt, M., 2003. Holocene paleoclimatic reconstruction based on the Lagoa Dourada deposits, southern Brazil. Geologica Acta: an international Earth science journal 1, 289-302.

Melo, M.S.d., Coimbra, A.M., 1996. Ruiniform relief in sandstones: the example of Vila Velha, Carboniferous of the Parana Basin, Southern Brazil. Acta Geologica Hispanica 31, 25-40.

Melo, M.S.d., Giannini, P.C.F., 2007. Sandstone dissolution landforms in the Furnas Formation, southern Brazil. Earth Surface Processes and Landforms 32, 2149-2164. http://dx.doi.org/10.1002/esp.1520

Merkel, A., 2020. Climate data of Ponta Grossa, Brasil www.climate-data.org/suedamerika/brasilien/parana/ponta-grossa-4493/.

Meyers, P.A., Teranes, J.L., 2001. Sediment Organic Matter, in: Last, W.M., Smol, J.P. (Eds.), Tracking Environmental Change Using Lake Sediments. Volume 2: Physical and Geochemical Methods. Kluwer Academic Publishers, Dordrecht, pp. 239-269.

Moro, R.S., de Mattos Bicudo, C.E., de Melo, M.S., Schmitt, J., 2004. Paleoclimate of the late Pleistocene and Holocene at Lagoa Dourada, Paraná State, southern Brazil. Quatern Int 114, 87-99. http://dx.doi.org/10.1016/s1040-6182(03)00044-2

Moro, R.S., Fürstenberger, C.B., 1998. Inferring lakewater characteristics in Lagoa Dourada, PR, Brazil, from surface sediment diatom assemblage data. Internationale Vereinigung für theoretische und angewandte Limnologie: Verhandlungen 26, 1755-1757. http://dx.doi.org/10.1080/03680770.1995.11901037

Morrill, C., LeGrande, A.N., Renssen, H., Bakker, P., Otto-Bliesner, B.L., 2013. Model sensitivity to North Atlantic freshwater forcing at 8.2 ka. Clim Past 9, 955–968.

Müller, P.J., Schneider, R., 1993. An automated leaching method for the determination of opal in sediments and particulate matter. Deep Sea Research Part I: Oceanographic Research Papers 40, 425-444.

Myers, N., Mittermeier, R.A., Mittermeier, C.G., Fonseca, G.A.B.d., Kent, J., 2000. Biodiversity hotspots for conservation priorities. Nature 403, 853–858.

Nesje, A., Søgnen, K., Elgersma, A., Dahl, S.O., 1987. A Piston Corer for Lake Sediments. Norsk Geografisk Tidsskrift - Norwegian Journal of Geography 41, 123-125. http://dx.doi.org/https://doi.org/10.1080/00291958708621986

Novello, V.F., Cruz, F.W., Vuille, M., Strikis, N.M., Edwards, R.L., Cheng, H., Emerick, S., de Paula, M.S., Li, X., Barreto, E.S., Karmann, I., Santos, R.V., 2017. A high-resolution history of the South American Monsoon from Last Glacial Maximum to the Holocene. Sci Rep 7, 44267. http://dx.doi.org/10.1038/srep44267

Novello, V.F., William da Cruz, F., Vuille, M., Pereira Silveira Campos, J.L., Stríkis, N.M., Apaéstegui, J., Moquet, J.S., Azevedo, V., Ampuero, A., Utida, G., Wang, X., Paula-Santos, G.M., Jaqueto, P., Ruiz Pessenda, L.C., Breecker, D.O., Karmann, I., 2021. Investigating δ13C values in stalagmites from tropical South America for the last two millennia. Quaternary Sci Rev 255. http://dx.doi.org/10.1016/j.quascirev.2021.106822

Nowaczyk, N.R., 2001. Logging of magnetic susceptibility, in: Last, W.M., Smol, J.P. (Eds.), Tracking environmental changes using lake sediments. Volume 1: Basin analysis, coring, and chronological techniques. Kluwer Academic Publishers, Dordrecht, The Netherlands, pp. 155-170.

Pedregosa, F., Varoquaux, G., Gramfort, A., Michel, V., Thirion, B., Grisel, O., Blondel, M., 2011. Scikit-Learn: Machine Learning in Python. Journal of Machine Learning Research 12, 2825–2830.

Piraquive Bermúdez, D., 2020. Vegetation and fire history in Araucaria forest and grasslands, southern Brazil. University of Göttingen, Göttingen, p. 144.

Piraquive Bermúdez, D., Theuerkauf, M., Giesecke, T., 2021. Towards quantifying changes in forest cover in the Araucaria forest-grassland mosaic in southern Brazil. Vegetation History and Archaeobotany. http://dx.doi.org/https://doi.org/10.1007/s00334-021-00841-2

Pires, L.F., Melo, M.S.d., Borges, J.A.R., Heck, R.J., Facin, P.C., 2019. X-ray Microtomography to Quantify Morphological Sandstones Properties. Brazilian Archives of Biology and Technology 62, e19180125. http://dx.doi.org/10.1590/1678-4324-2019180125

Pontes, H., Fernandes, L., de Melo, M., Guimarães, G., Massuqueto, L., 2020. Speleothems in quartz-sandstone caves of Ponta Grossa municipality, Campos Gerais region, Paraná state, southern Brazil. International Journal of Speleology 49, 119-136. http://dx.doi.org/10.5038/1827-806x.49.2.2313

Portes, M.C.G.d.O., Safford, H., Behling, H., 2018. Humans and climate as designers of the landscape in Serra da Bocaina National Park, southeastern Brazil, over the last seven centuries. Anthropocene 24, 61-71. http://dx.doi.org/10.1016/j.ancene.2018.11.004

Rodrigues-Filho, S., Behling, H., Irion, G., Müller, G., 2002. Evidence for Lake Formation as a Response to an Inferred Holocene Climatic Transition in Brazil. Quaternary Research 57, 131-137. http://dx.doi.org/10.1006/qres.2001.2281

Rothwell, R.G., 1989. The Smear Slide Method - An Optical Identification Guide. Springer, Dordrecht. https://doi.org/10.1007/978-94-009-1133-8_2

Suguio, K., Turcq, B., Servant, M., Soubiös, F., Foumier, M., 1989. Holocene fluvial deposits in southeastem Brazil: chronology and palaeohydrological implications, International Symposium on Global Changes in South America During the Quatemary, 7G-73, Säo Paulo (Brazil), pp. 70-74.

Thomaz, G.M., 2010. Vila Velha State Park, Brazil: Curious and Very Interesting Sandstone Formations, pp. https://traveltoparana.wordpress.com/2010/2005/2006/parque-estadual-de-vila-velha-state-park-parana-brazil/.

Tjallingii, R., Röhl, U., Kölling, M., Bickert, T., 2007. Influence of the water content on X-ray fluorescence core-scanning measurements in soft marine sediments. Geochemistry, Geophysics, Geosystems 8, 1-12. http://dx.doi.org/doi:10.1029/2006GC001393

Utida, G., Cruz, F.W., Santos, R.V., Sawakuchi, A.O., Wang, H., Pessenda, L.C.R., Novello, V.F., Vuille, M., Strauss, A.M., Borella, A.C., Stríkis, N.M., Guedes, C.C.F., Dias De Andrade, F.R., Zhang, H., Cheng, H., Edwards, R.L., 2020. Climate changes in Northeastern Brazil from deglacial to Meghalayan periods and related environmental impacts. Quaternary Sci Rev 250, 106655. http://dx.doi.org/10.1016/j.quascirev.2020.106655

van der Walt, S., Schönberger, J., Nunez-Iglesias, J., Boulogne, F., Warner, J., Yager, N., Gouillart, E., Yu, T., the scikit-image contributors, 2014. scikit-image: image processing in Python. PeerJ 2, e453. http://dx.doi.org/https://doi.org/10.7717/peerj.453

Virtanen, P., Gommers, R., Oliphant, T.E., Haberland, M., Reddy, T., Cournapeau, D., Burovski, E., Peterson, P., Weckesser, W., Bright, J., van der Walt, S.J., Brett, M., Wilson, J., Millman, K.J., Mayorov, N., Nelson, A.R.J., Jones, E., Kern, R., Larson, E., Carey, C.J., Polat, İ., Feng, Y., Moore, E.W., VanderPlas, J., Laxalde, D., Perktold, J., Cimrman, R., Henriksen, I., Quintero, E.A., Harris, C.R., Archibald, A.M., Ribeiro, A.H., Pedregosa, F., van Mulbregt, P., Vijaykumar, A., Bardelli, A.P., Rothberg, A., Hilboll, A., Kloeckner, A., Scopatz, A., Lee, A., Rokem, A., Woods, C.N., Fulton, C., Masson, C., Häggström, C., Fitzgerald, C., Nicholson, D.A., Hagen, D.R., Pasechnik, D.V., Olivetti, E., Martin, E., Wieser, E., Silva, F., Lenders, F., Wilhelm, F., Young, G., Price, G.A., Ingold, G.-L., Allen, G.E., Lee, G.R., Audren, H., Probst, I., Dietrich, J.P., Silterra, J., Webber, J.T., Slavič, J., Nothman, J., Buchner, J., Kulick, J., Schönberger, J.L., de Miranda Cardoso, J.V., Reimer, J., Harrington, J., Rodríguez, J.L.C., Nunez-Iglesias, J., Kuczynski, J., Tritz, K., Thoma, M., Newville, M., Kümmerer, M., Bolingbroke, M., Tartre, M., Pak, M., Smith, N.J., Nowaczyk, N., Shebanov, N., Pavlyk, O., Brodtkorb, P.A., Lee, P., McGibbon, R.T., Feldbauer, R., Lewis, S., Tygier, S., Sievert, S., Vigna, S., Peterson, S., More, S., Pudlik, T., Oshima, T., Pingel, T.J., Robitaille, T.P., Spura, T., Jones, T.R., Cera, T., Leslie, T., Zito, T., Krauss, T., Upadhyay, U., Halchenko, Y.O., Vázquez-Baeza, Y., SciPy, C., 2020. SciPy 1.0: fundamental algorithms for scientific computing in Python. Nature Methods 17, 261-272. http://dx.doi.org/10.1038/s41592-019-0686-2

Wang, X., Auler, A.S., Edwards, R.L., Cheng, H., Ito, E., Wang, Y., Kong, X., Solheid, M., 2007. Millennial-scale precipitation changes in southern Brazil over the past 90,000 years. Geophys Res Lett 34, n/a-n/a. http://dx.doi.org/10.1029/2007gl031149

Weltje, G., Bloemsma, M., Tjallingii, R., Heslop, D., Röhl, U., Croudace, I., 2015. Prediction of Geochemical Composition from XRF Core Scanner Data: A New Multivariate Approach Including Automatic Selection of Calibration Samples and Quantification of Uncertainties, in: Croudace, I., Rothwell, R. (Eds.), Micro-XRF Studies of Sediment Cores. Springer, Dordrecht, pp. 507-534. https://doi.org/10.1007/978-94-017-9849-5_21

Weltje, G.J., Tjallingii, R., 2008. Calibration of XRF core scanners for quantitative geochemical logging of sediment cores: Theory and application. Earth and Planetary Science Letters 274, 423-438. http://dx.doi.org/10.1016/j.epsl.2008.07.054

Woodward, C.A., Gadd, P.S., 2019. The potential power and pitfalls of using the X-ray fluorescence molybdenum incoherent: Coherent scattering ratio as a proxy for sediment organic content. Quatern Int 514, 30-43. http://dx.doi.org/10.1016/j.quaint.2018.11.031

Wray, R.A.L., 2013. Solutional weathering and karstic landscapes on quartz sandstones and quartzite, in: Frumkin, A. (Ed.), Treatise on Geomorphology. Academic Press, San Diego, pp. 463-483.

Wright, H.E., 1967. A square-rod piston sampler for lake sediments. Journal of Sedimentary Research 37, 975-976. http://dx.doi.org/https://doi.org/10.1306/74D71807-2B21-11D7-8648000102C1865D

Zhou, J., Lau, K.-M., 1998. Does a Monsoon Climate Exist over South America? J Climate 11, 1020-1040.

Zolitschka, B., 1998. A 14,000 year sediment yield record from Western Germany based on annually laminated sediments. Geomorphology 22, 1-17.

Zolitschka, B., Fey, M., Janssen, S., Maidana, N.I., Mayr, C., Wulf, S., Haberzettl, T., Corbella, H., Lücke, A., Ohlendorf, C., Schäbitz, F., 2019. Southern Hemispheric Westerlies control sedimentary processes of Laguna Azul (south-eastern Patagonia, Argentina). The Holocene 29, 403-420. http://dx.doi.org/10.1177/0959683618816446

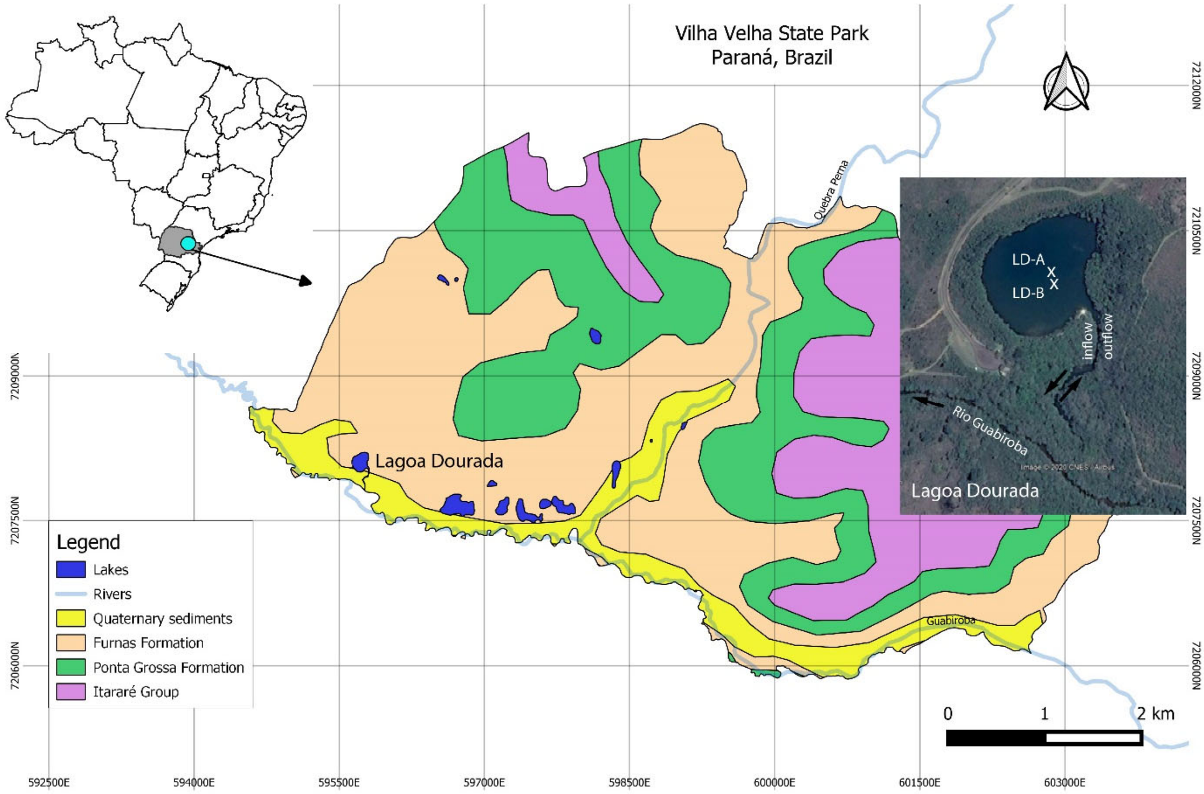

Fig. 1: Location of Lagoa Dourada in Paraná (South Brazil) with a geological map of the Vilha Velha State Park based on information from “Plano de Manejo Vegetacao Parque Estadual Vila Velha” (Goberno do Estado de Paraná, 2004) and an aerial photography of the lake with Rio Guabiroba from Google Earth.

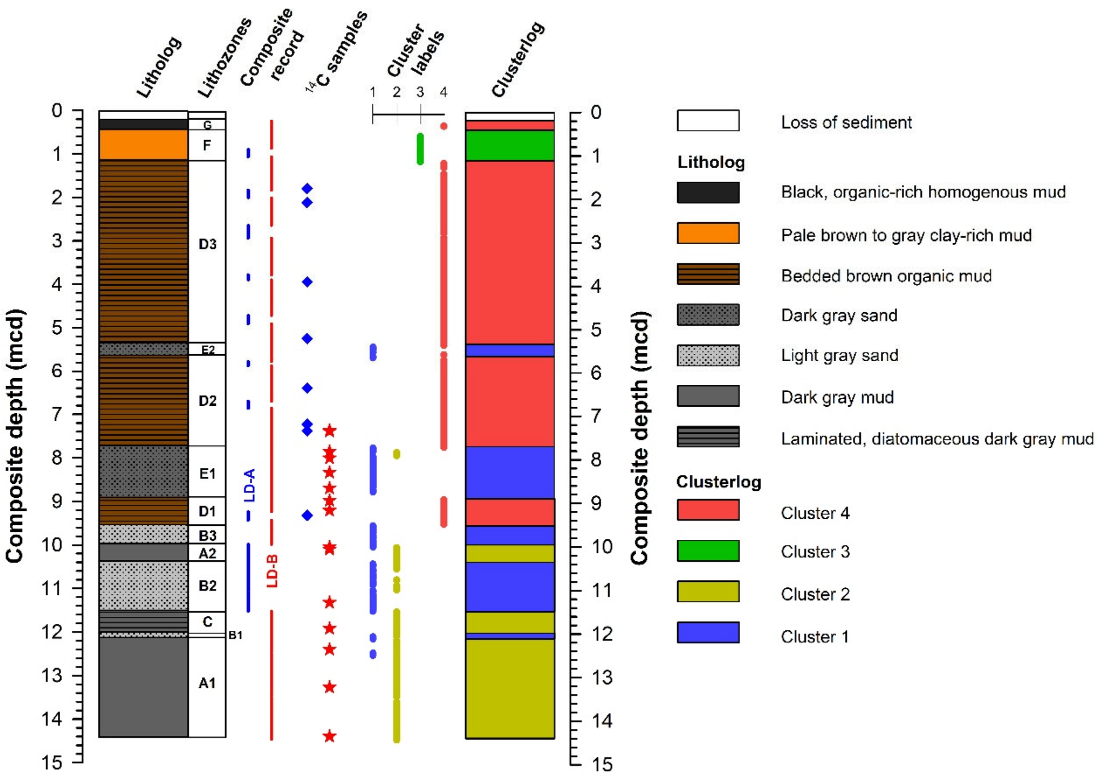

Fig. 2: Litholog (left) of the composite record based on macroscopic and microscopic observations with lithozones A1 through G, core sections used for the construction of the composite record as well as positions of samples for radiocarbon (^{14}C) dating. Clusterlog (right) based on cluster analysis for comparison.

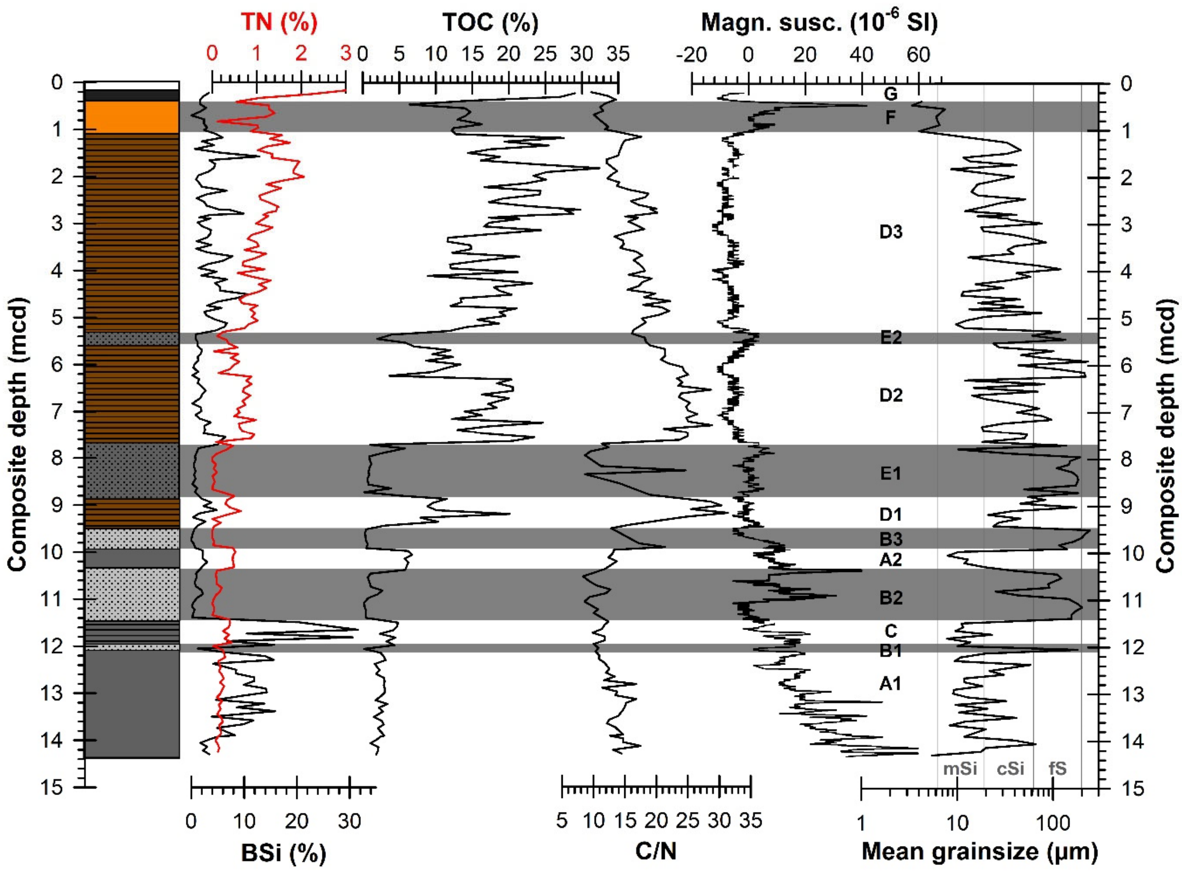

Fig. 3: Litholog with lithozones A1 through G (for legend: cf., Fig. 2) with bulk geochemistry, including total nitrogen (TN), total organic carbon (TOC), magnetic susceptibility (magn. susc.), biogenic silica (BSi), carbon-to-nitrogen ratio (C/N) and mean grainsize. Sand horizons (LZs B and E) and lithozone F are shaded in gray.

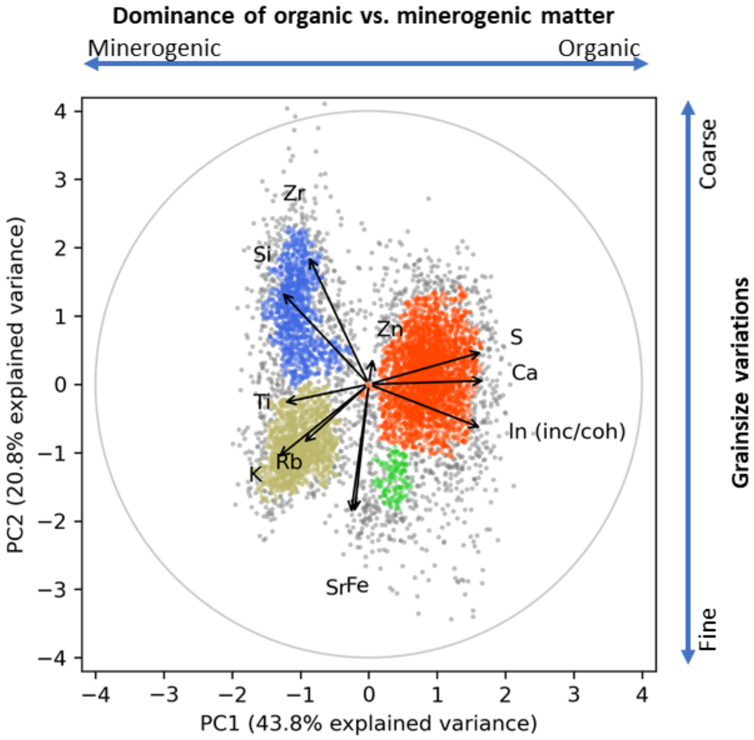

Fig. 4: PCA loadings from homogenized (clr-transformed) elemental intensities obtained by XRF core scanning. The first two principal components preserve 64.6 % of the total variance. The four determined clusters (Cluster 1-4) are color-coded (for legend: cf., Fig. 2) and data points related to noise are plotted in gray. The circle indicates a value of 1 for the loadings. Interpretations in terms of grainsize variations and dominance of organic vs. minerogenic matter are indicated by blue arrows.

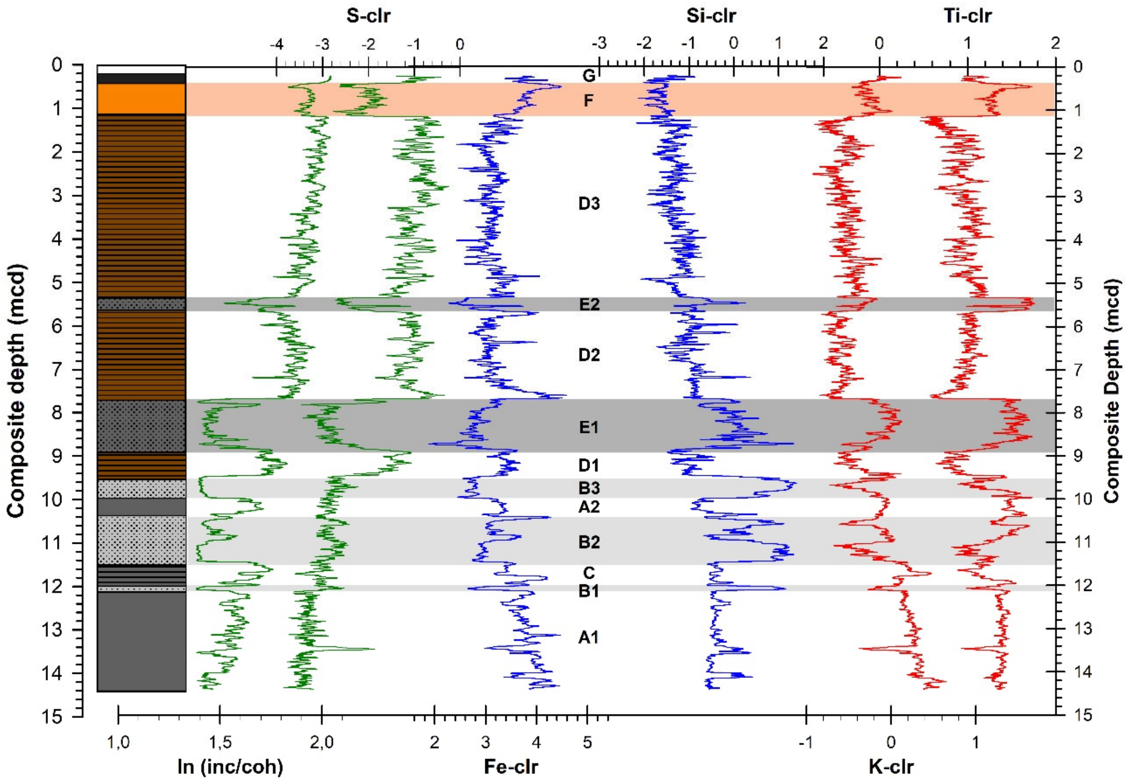

Fig. 5: Litholog with lithozones A1 through G (for legend: cf., Fig. 2) and selected clr-transformed elemental data obtained by XRF core scanning. Shown are the elements sulphur (S), silica (Si), titanium (Ti), iron (Fe), potassium (K) and the incoherent/coherent ratio (inc/coh). Sand horizons (LZs B and E) and lithozone F are shaded in gray.

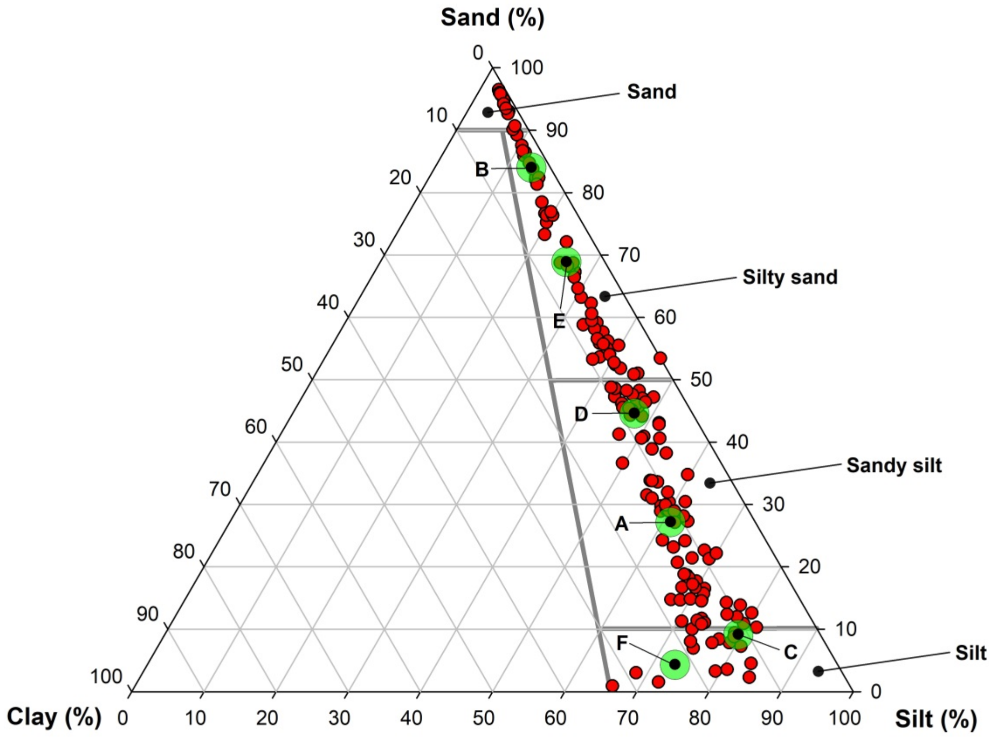

Fig. 6: Ternary grainsize diagram (red dots mark individual samples) with mean grainsize values for lithozones A-F (labeled with the corresponding letter and encircled in green color).

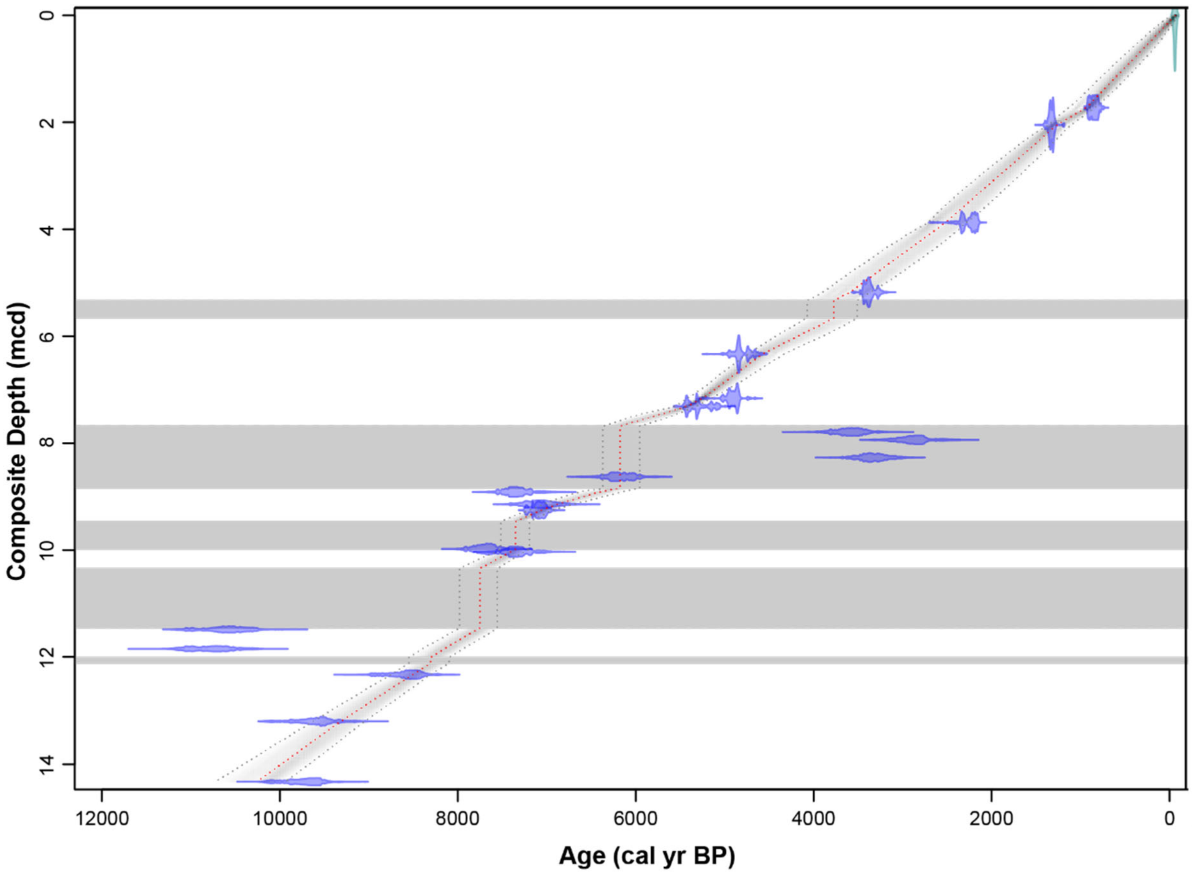

Fig. 7: Age-depth relationship (red dotted line) modelled with “rbacon” and based on 21 radiocarbon dates (in blue) with the sediment surface (in green). The 1σ error margins (gray dotted lines) are indicated as well as the five sand horizons (gray horizontal bars) excluded from age-depth model calculations.

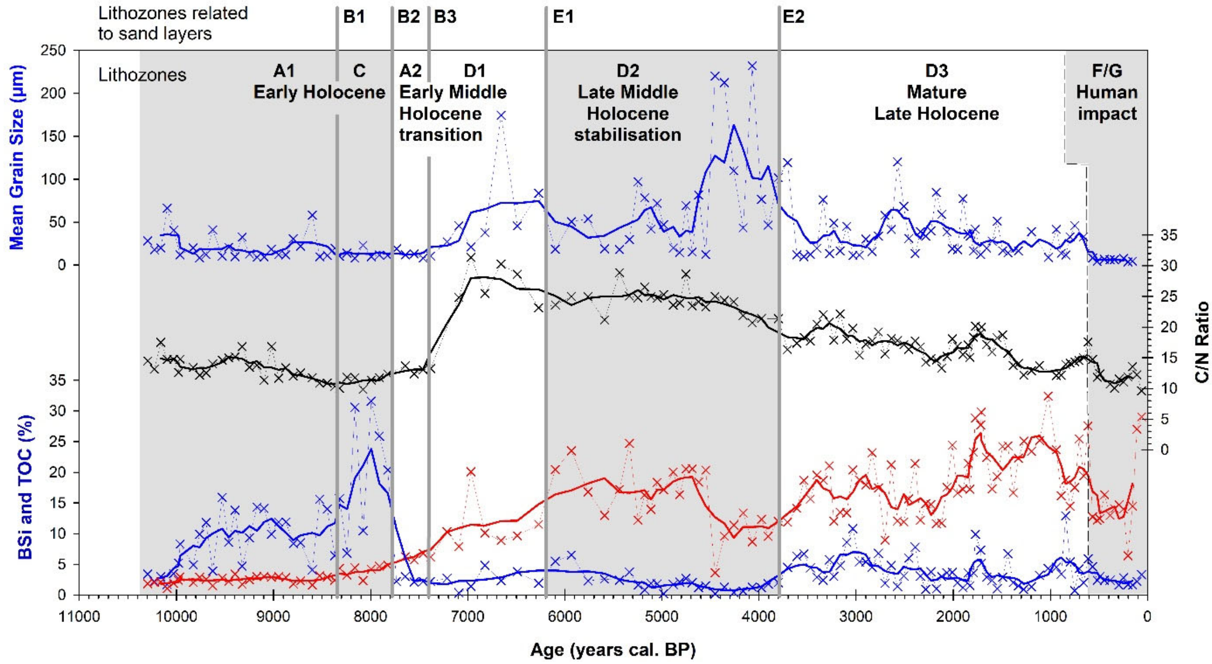

Fig. 8: Selected geochemical data (biogenic silica: BSi; total organic carbon: TOC; carbon-to-nitrogen ratio: C/N ratio) are shown together with mean grainsize vs. time. Lithozones and the position of excluded sand horizons (LZs B and E) are labelled. Additionally, stratigraphical assignments and human impact are labeled.

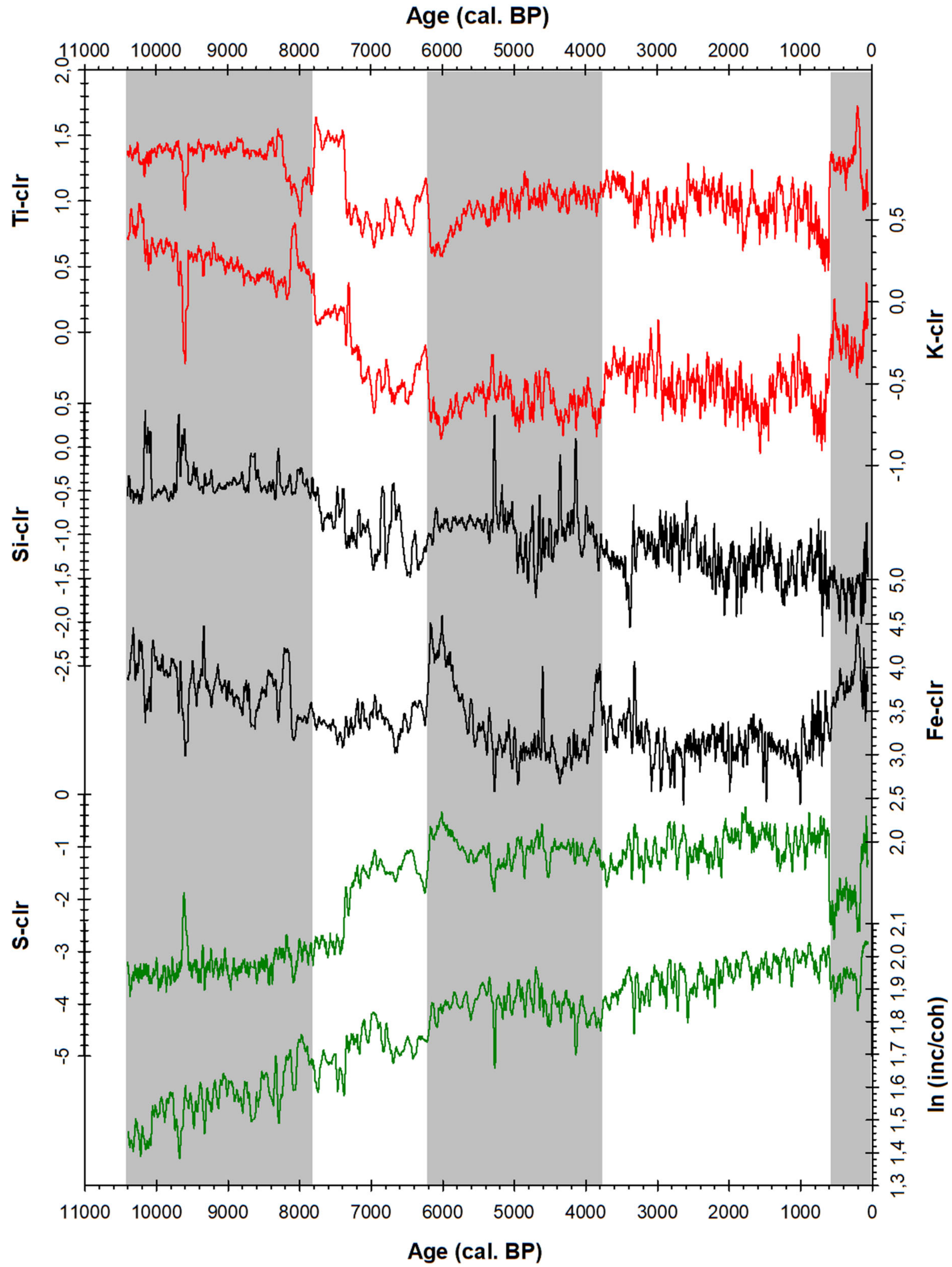

Fig. 9: Selected clr-transformed elemental data obtained by XRF core scanning. Shown are the elements sulphur (S), silica (Si), titanium (Ti), potassium (K), iron (Fe) and the incoherent/coherent ratio (inc/coh) vs. time. Shading as in Fig. 8.

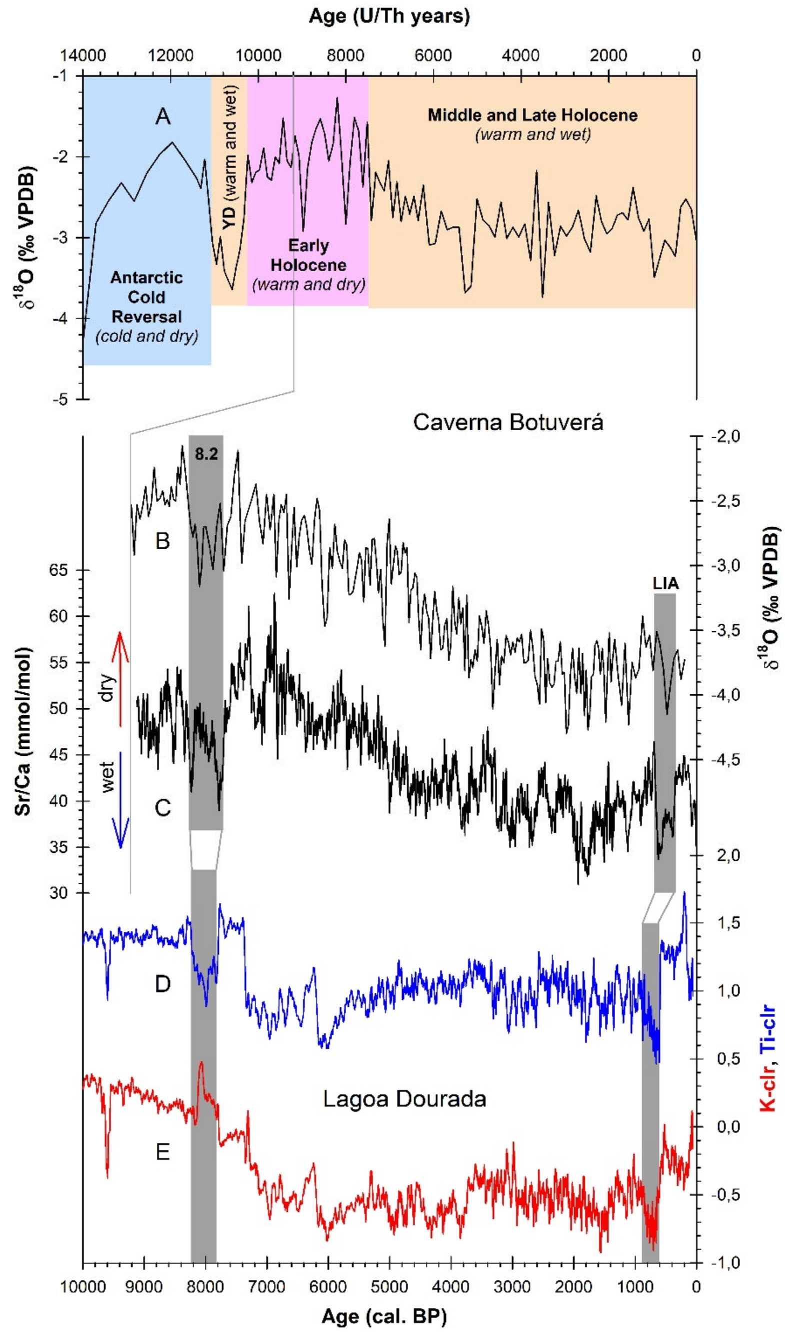

Fig. 10: Comparison of speleothem data from Caverna Botuverá with lacustrine sediment data from Lagoa Dourada. A) Oxygen isotope record from Botuverá speleothem BTV2 focusing on the last 14 ka (Cruz, 2005; Cruz et al., 2005). Climatic conditions are labelled and color-coded (YD: Younger Dryas) and derived from Novello et al. (2017). Note: the time scale is in U/Th years! B) Oxygen isotope record and C) Sr/Ca ratio from Botuverá speleothem BTV21 for the Holocene (Bernal et al., 2016a; Bernal et al., 2016b) with hydroclimatic interpretation (arrows). Additionally, clr-transformed elemental data of Ti (D) and K (E) are shown from the sediment record of Lagoa Dourada. The two most prominent Holocene climatic events are marked with vertical gray bars. Note: the chronology for the last millennium of the Lagoa Dourada record is shown with the "rbacon" age-depth model causing a temporal offset for the last millennium – for explanation: see the text. All data from Caverna Botuverá were accessed online via the NOAA Paleoclimatology Program on February 18, 2021.

Tab. 1: Radiocarbon ages with sample depths, sample characteristics as well as reservoir correction. Ages used for calculation of the reservoir effect are excluded from age-depth modelling (shaded in dark gray) as well as outliers mainly located in sand horizons (shaded in light gray).

Sample ID (LD-)	Lab. No.	Sampled Core	Section Depth (cm)	Composit Depth (mcd)	Radiocarbon Age (BP)	± 1 σ	Type of Sample	Reservoir Correction (yrs)	Comments
1	POZ-119117	LD-B2	89.5-90.5	1,726	990	30	Macro-fossil		
2	POZ-111295	LD-B3	29-30	2,048	1470	30	Macro-fossil		
3	UBA-29240	LD-B5	6.8-6.9	3,873	2330	35	Macro-fossil		
4	POZ-121537	LD-B6	41-42	5,177	3205	35	Macro-fossil		
5	POZ-119118	LD-B7	56.2-56.6	6,332	4300	35	Macro-fossil		
6	POZ-107807	LD-B8	39.1-39.2	7,161	4355	35	Macro-fossil		
7	POZ-122526	LD-B8	53-54	7,3	9700	40	Bulk	5065	age used for reservoir correction with LD-8
8	POZ-119119	LD-B8	54.1-54.5	7,311	4635	35	Macro-fossil		
9	POZ-119120	LD-B8	55-56	7,32	9870	40	Bulk	5235	age used for reservoir correction with LD-8
10	POZ-122527	LD-B8	102-103	7,79	8530	50	Bulk		outlier; from sand horizon
11	POZ-119121	LD-B9	10-11	7,938	7930	50	Bulk		outlier; from sand horizon
12	POZ-116232	LD-B9	43-44	8,268	8330	40	Bulk		outlier; from sand horizon
13	POZ-122528	LD-B9	79-80	8,628	10590	50	Bulk		from sand horizon
14	POZ-119122	LD-B10	41-42	8,912	11630	60	Bulk		
15	POZ-111296	LD-B10	64-65	9,142	11380	60	Bulk	5145	age used to test reservoir correction with LD-16
16	UBA-29241	LD-B10Liv	9.3-9.8	9,252	6235	35	Macro-fossil		
17	POZ-107808	LD-B10Liv	82-83	9,979	12020	60	Bulk		
18	POZ-119188	LD-A11	29-30	10,03	11620	50	Bulk		
19	POZ-107809	LD-B11	96-97	11,255	14540	80	Bulk		outlier; from sand horizon
20	POZ-116234	LD-B12	42-43	11,85	14660	80	Bulk		outlier
21	POZ-111297	LD-B12	90-91	12,33	12930	60	Bulk		
22	POZ-107810	LD-B 13	76-77	13,2	13750	70	Bulk		
23	POZ-107815	LD-B 14	97-98	14,326	13850	70	Bulk		
	POZ: Poznań Radiocarbon Laboratory, Poland								
	UBA: ^{14}Chrono Centre at Queen's University Belfast, Northern Ireland								

Supplementary Material

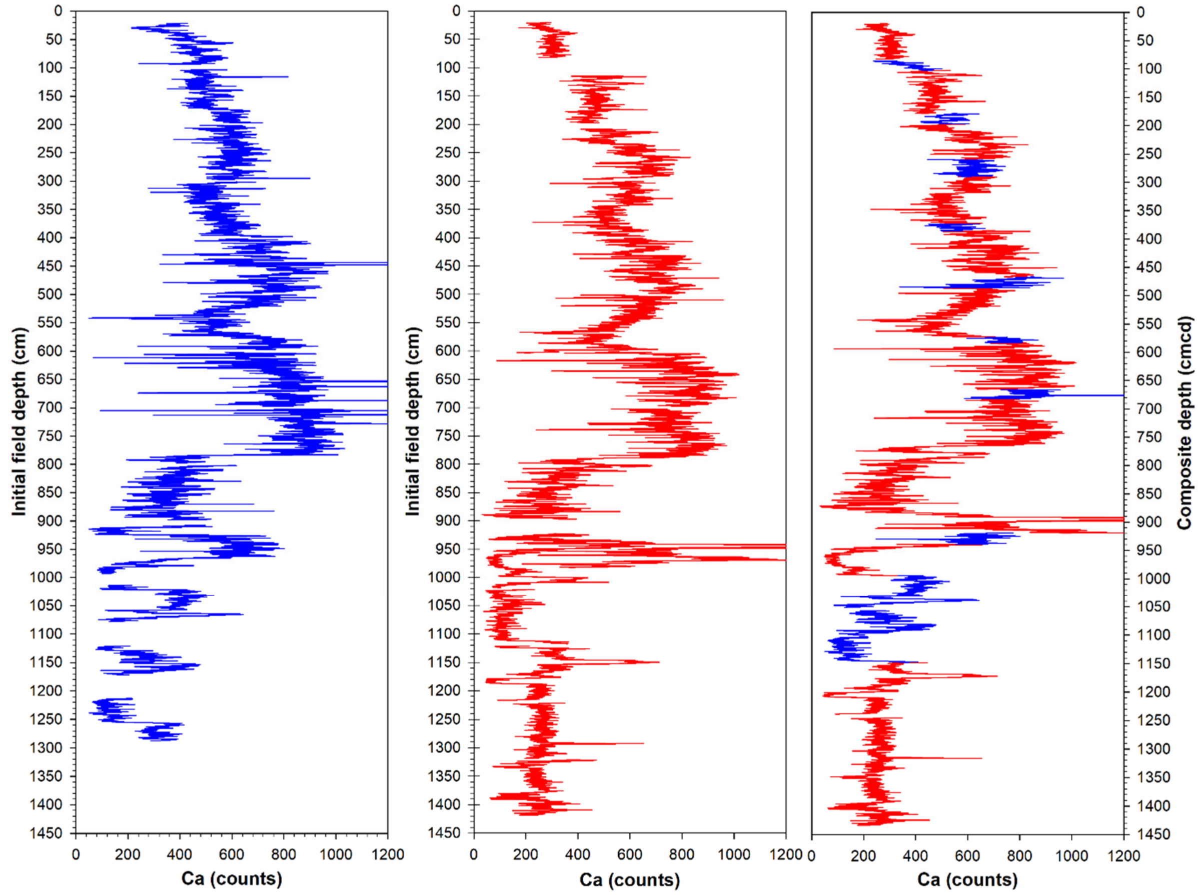

Fig. S1: Ca counts obtained by XRF core scanning vs. field depths for sediment cores LD17-A (blue) and LD17-B (red) as well as for the merged composite record, now on a composite depth scale and displayed in centimeter composite depth (cmcd).

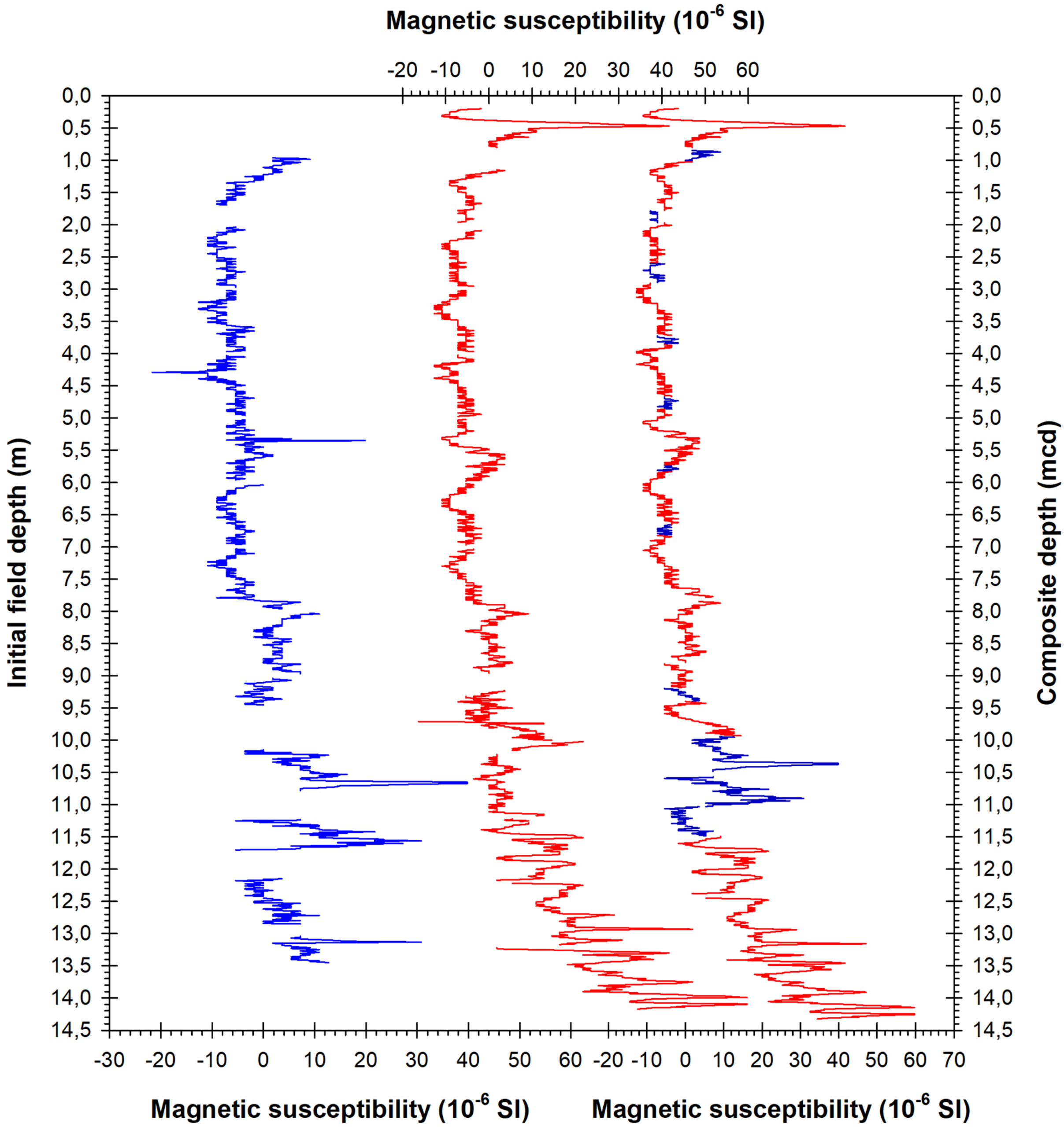

Fig. S2: Magnetic susceptibility versus field depths for sediment cores LD17-A (blue) and LD17-B (red) as well as for the merged composite record displayed on a composite depth scale in meter composite depth (mcd). Correlation of LD17-A and LD17-B is not based on the magnetic susceptibility data shown but on Ca data (cf., Fig. S1).

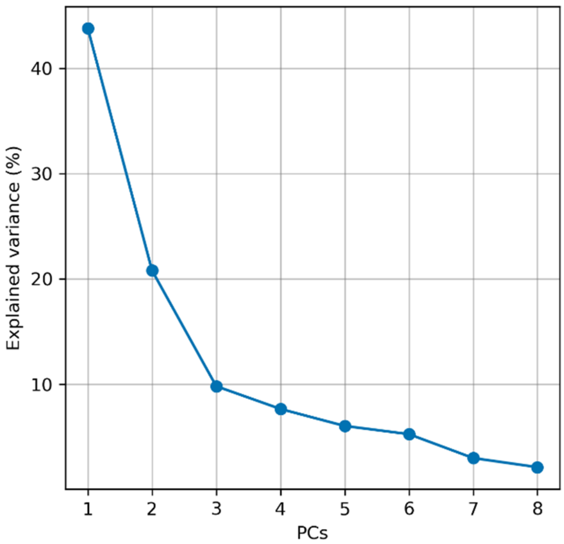

Fig. S3: Scree plot of the explained variance ratio for all principal components (PCs) based on normalized (clr-transformed) and standardized elemental intensities obtained by XRF core scanning (cf., Fig. 4).

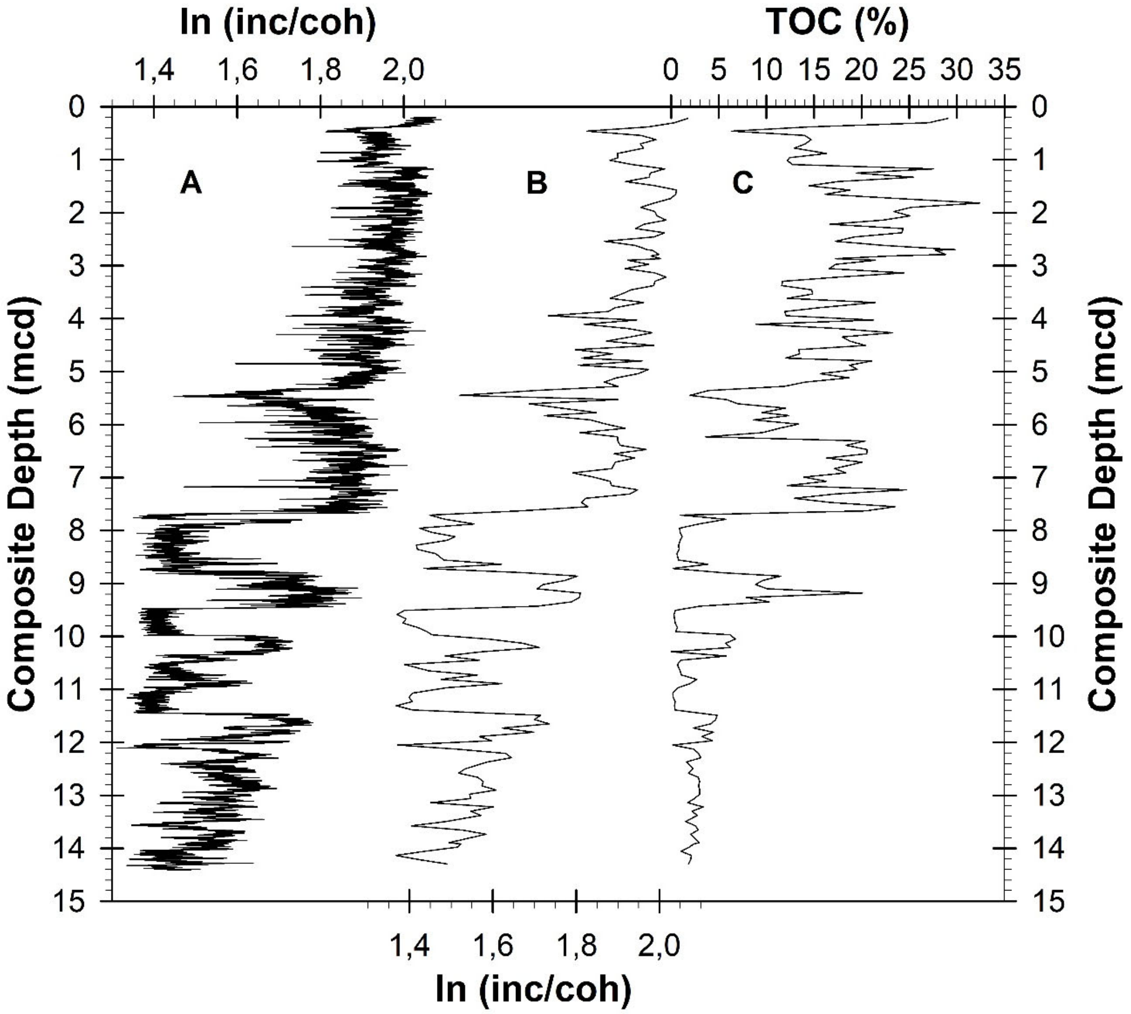

Fig. S4: Organic matter for the sediment record from Lagoa Dourada. A) High resolution (2 mm) record of the ln inc/coh ratio; B) Same ratio with resolution reduced to 8 cm; C) Low resolution (8 cm) total organic carbon (TOC) record. Correlation between B and C: r = 0.88.

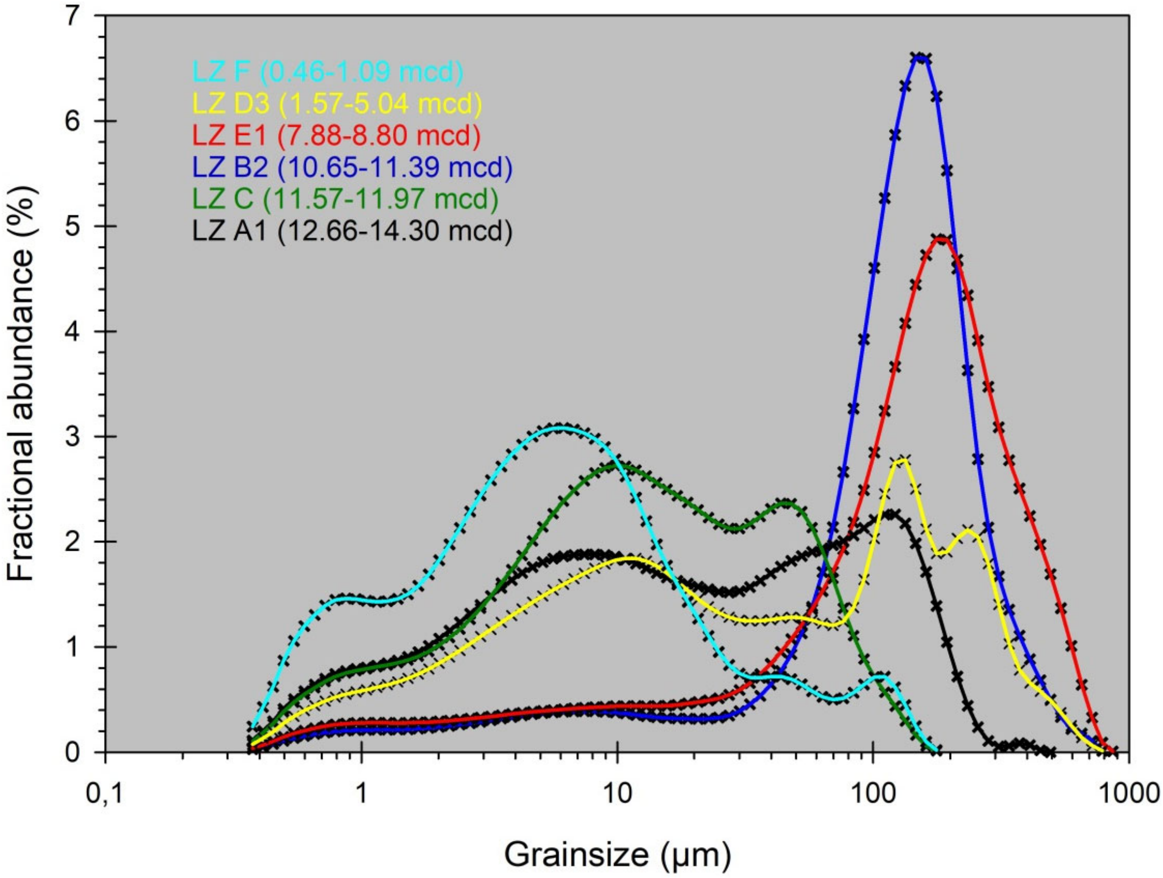

Fig. S5: Grainsize frequency histograms of mean distributions for selected lithozones.

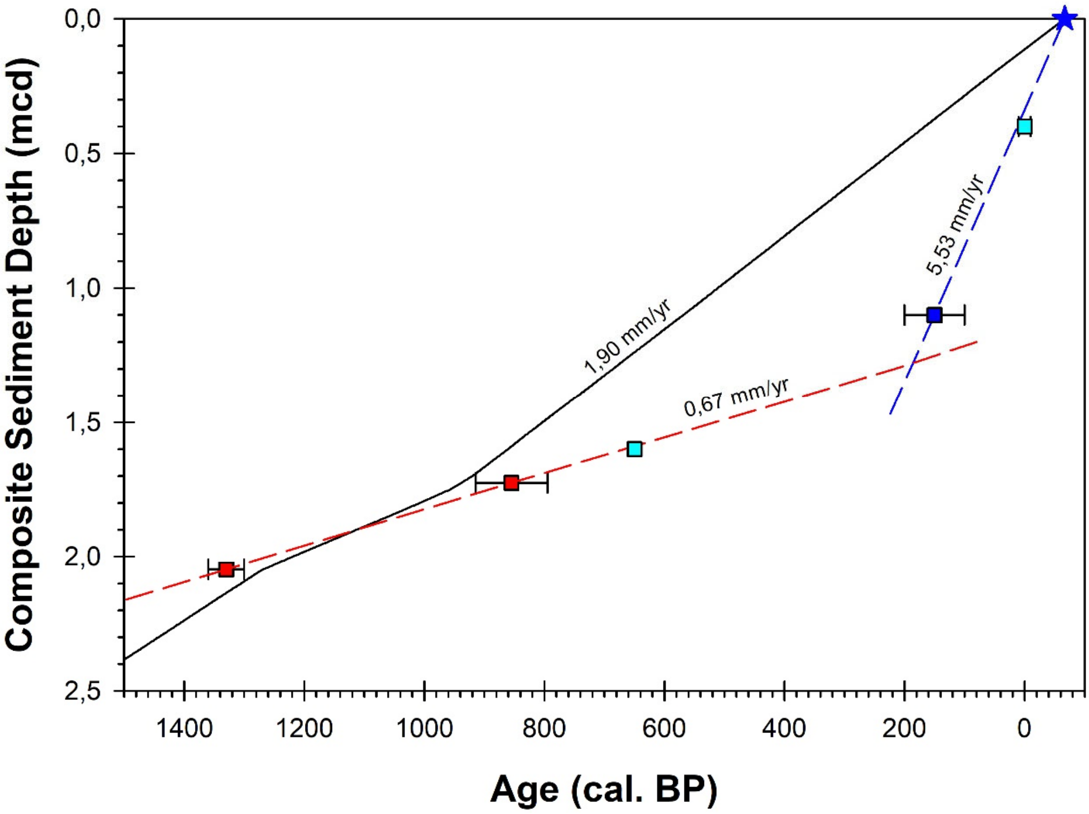

Fig. S6: Modified chronology for the last 1500 years. On display are the “rbacon” age-depth model (black line), the two uppermost radiocarbon ages (red squares) with a linear sedimentation rate based on these two dates only (red dashed line) and an age for the onset of deforestation (AD 1800 ±50 years: blue square) with a linear sedimentation rate (blue dashed line) calculated for this historical date and the sediment surface of the year of coring, i.e. AD 2017 (blue asterisk). Values provided in mm/yr are respective linear sedimentation rates. Additionally, two data points are shown (cyan): (1) AD 1953 at 0.4 mcd, the year of establishing the Vila Velha State Park as indicated by returning organic sediments (onset of LZ G) coinciding with the calculated linear sedimentation rate; (2) The change in elemental data at 1.6 mcd interpreted as the onset of the LIA (see text for explanation) and its timing of AD 1300 (650 cal. BP) as based on linearly extrapolating the radiocarbon-based sedimentation rates.

Tab. S1: Correlation coefficients for 20 elements as well as incoherent (inc) and coherent (coh) radiation analyzed with the XRF core scanner for sediment cores LD-B6 (organic) and LD-B12 (minerogenic). Both cores were 97 cm in length, scanned every 2 mm and consist of 486 individual data points. Each core scanning was repeated five times. Only elements with a high positive correlation of r > 0.8 for at least one of the two core sections (shaded in gray) were selected for further statistical treatment.

LD-B6																						
Element	Al	Si	P	S	Cl	K	Ca	Ti	V	Cr	Mn	Fe	Ni	Cu	Zn	Br	Rb	Sr	Zr	Pb	Inc	Coh
Mean counts for each element	35	149	17	135	7	217	1115	1248	24	74	28	9075	167	174	145	41	133	160	1044	43	51666	8473
Correlation coefficient	0,052	0,956	0,037	0,994	0,037	0,941	1,000	0,997	0,183	0,360	0,350	0,999	0,273	0,396	0,860	0,158	0,523	0,519	0,981	0,127	0,995	0,902
P value	0,288	<0,00001	0,6028	0	0,428	<0,00001	0	0	0,00003	<0,00001	<0,00001	0	<0,00001	<0,00001	<0,00001	0,00036	<0,00001	<0,00001	0	0,00311	0	0

LD-B12																						
Element	Al	Si	P	S	Cl	K	Ca	Ti	V	Cr	Mn	Fe	Ni	Cu	Zn	Br	Rb	Sr	Zr	Pb	Inc	Coh
Mean counts for each element	54	532	24	29	13	675	295	2043	25	53	34	21607	148	152	204	23	377	430	1687	102	39096	7919
Correlation coefficient	0,094	0,978	-0,003	0,137	0,036	0,983	0,966	0,993	0,140	0,297	0,715	0,999	0,344	0,476	0,641	0,329	0,853	0,922	0,992	0,505	0,991	0,734
P value	0,0321	0	0,4103	0,0019	0,2135	0	<0,00001	0	0,00098	<0,00001	<0,00001	0	<0,00001	<0,00001	<0,00001	<0,00001	<0,00001	<0,00001	0	<0,00001	0	<0,00001